

1 **New and Updated Global Empirical Seawater Property Estimation Routines**

2 Carter, B. R.^{1,2}, Bittig, H. C.³, Fassbender, A. J.², Sharp, J. D.^{1,2}, Takeshita, Y.⁴, Xu, Y.-Y.^{5,6},
3 Álvarez, M.⁷, Wanninkhof, R.⁶, Feely, R. A.², Barbero, L.^{5,6}

4 ¹Cooperative Institute for Climate, Oceans, and Ecosystems, University of Washington, Seattle, WA,
5 98195

6 ²Pacific Marine Environmental Laboratory, 7600 Sand Point Way, NE, Seattle, WA, 98195

7 ³Leibniz Institute for Baltic Sea Research Warnemünde, Dept. of Marine Chemistry, Seestraße 15, 18119
8 Rostock-Warnemünde, Germany

9 ⁴Monterey Bay Aquarium Research Institute, 7700 Sandholdt Road, Moss Landing, CA 95039

10 ⁵Cooperative Institute for Marine and Atmospheric Studies, Rosenstiel School of Marine and
11 Atmospheric Science, 4600 Rickenbacker Causeway, University of Miami, Miami, FL, 33149

12 ⁶Atlantic Oceanographic and Meteorological Laboratory, 4301 Rickenbacker Causeway, Miami, FL,
13 33149

14 ⁷Instituto Español de Oceanografía, A Coruña, 15001, Spain

15 *Correspondence to:* Brendan Carter (brcarter@uw.edu)

16 **Abstract**

17 We introduce three new Empirical Seawater Property Estimation Routines (ESPERs) capable of
18 predicting seawater phosphate, nitrate, silicate, oxygen, total titration seawater alkalinity (TA),
19 total hydrogen scale pH (pH_T), and total dissolved inorganic carbon (DIC) from up to 16
20 combinations of seawater property measurements. The routines generate estimates from neural
21 networks (ESPER_NN), locally-interpolated regressions (ESPER_LIR), or both
22 (ESPER_Mixed). They require a salinity value and coordinate information, and benefit from
23 additional seawater measurements if available. These routines are intended for seawater
24 property measurement quality control and quality assessment, generating estimates for
25 calculations that require approximate values, original science, and producing biogeochemical
26 property context from a data set. Relative to earlier LIR routines, the updates expand their
27 functionality, including new estimated properties and combinations of predictors, a larger
28 training data product including new cruises from the 2020 Global Data Analysis Project data
29 product release, and the implementation of a first-principles approach for quantifying the impacts
30 of anthropogenic carbon on DIC and pH_T . We show that the new routines perform at least as
31 well as existing routines, and, in some cases, outperform existing approaches, even when limited
32 to the same training data. Given that additional training data has been incorporated into these
33 updated routines, these updates should be considered an improvement over earlier versions. The
34 routines are intended for all ocean depths for the interval from 1980 to \sim 2030 c.e., and we
35 caution against using the routines to directly quantify surface ocean seasonality or make more
36 distant predictions of DIC or pH_T .

37

38

39

40

41

42

43 **1. Introduction**

44 Anthropogenic impacts on the environment are changing the physical and chemical state of the
45 ocean. The accumulation of excess ocean heat (Roemmich et al. 2012; Purkey and Johnson
46 2013) and carbon (Sabine et al. 2004; Khatiwala et al. 2013; Carter et al. 2017, 2019a; Gruber et
47 al. 2019) and the redistribution of freshwater between regions of the ocean (Durack et al. 2012)
48 and geological reservoirs are modifying ocean circulation pathways and causing sea level rise
49 (Nerem et al. 2018), ocean acidification (Feely et al. 2004, 2009; Doney et al. 2009; Jiang et al.
50 2019), and ocean deoxygenation (Sasano et al. 2018). These changes are fundamentally shifting
51 the physical and chemical environments of marine organisms and threatening ocean ecosystems
52 and services (Gattuso et al. 2015; Doney et al. 2020).

53 Global climate change poses a challenge for ocean monitoring, necessitating sustained high-
54 quality measurements across timescales and across the vast and remote global ocean. A variety
55 of approaches and platforms have been developed for ocean monitoring (e.g., autonomous
56 surface vehicles, profiling floats, and fixed moorings), each of which has a niche for examining a
57 range of temporal and spatial scales (Bushinsky et al. 2019) and each of which has strengths and
58 weaknesses for addressing aspects of global change (Carter et al. 2019b). The cost and difficulty
59 of measurements is a limiting factor for all approaches, so it is impossible as of today to have
60 extensive high-quality and high-frequency measurements everywhere they are desired. Given
61 this limitation, an emerging approach involves using algorithms that have been trained to
62 reproduce measurements of seawater properties from co-located measurements of other seawater
63 properties. These algorithms take advantage of strong regional correlations between seawater
64 properties that result from oceanographic processes that shape the distributions of many different
65 seawater properties in similar ways (e.g., organic matter cycling with nearly constant
66 stoichiometric ratios between macronutrients, and freshwater cycling that linearly dilutes or
67 concentrates most chemical concentrations in seawater). Once trained, the algorithms can be
68 used to predict the desired properties from other properties that are more routinely measured
69 either remotely by satellite or using available in situ sensors. This strategy has seen use for more
70 than two decades (e.g., Goyet et al. 2000; Lee et al. 2006), though recent advances in skill,
71 flexibility, and diversity of the algorithms available (Carter et al. 2016, 2018; Sauzède et al.
72 2017; Bittig et al. 2018; Landschützer et al. 2019; Gregor and Gruber 2021) have made it
73 possible to create climatologies (Broullón et al. 2019, 2020; Jiang et al. 2019), calibrate and
74 monitor drift-adjustments for sensors on autonomous sensor platforms (Johnson et al. 2017;
75 Takeshita et al. 2018), create novel global data products (Carter et al. 2021), and fill holes in data
76 sets when the final analysis is not strongly sensitive to estimate errors, e.g., when silicate and
77 phosphate are estimated for use in seawater carbonate chemistry calculations (e.g., van Hueven
78 et al. 2011) or when total alkalinity (TA) is needed to convert pH_T between temperatures (Carter
79 et al. 2019a; Jiang et al. 2019).

80 The growing number of use cases for seawater property estimation algorithms means it is
81 important to refine the algorithms to the extent possible, especially given that some observing

82 approaches depend on these algorithms for sensor calibration and validation. As a notable
83 example, biogeochemical Argo floats calibrate pH_T and nitrate sensors using algorithm estimates
84 in the comparatively stable mid-depths of the ocean (Johnson et al. 2017), and additionally rely
85 on estimated seawater alkalinity at all depths to calculate dissolved inorganic carbon (DIC) and
86 the partial pressure of CO_2 ($p\text{CO}_2$) (Williams et al. 2018; Gray et al. 2018).

87 Increasing ocean DIC content from anthropogenic carbon (C_{ant}) storage and decreasing pH_T
88 values from ocean acidification (OA) provide an ongoing challenge to the accuracy of these
89 algorithms: the algorithms are trained, or fit, to data collected over the last three decades, but will
90 be used primarily to estimate seawater properties specific to recent years and the coming years
91 until improved algorithms become available. How then should we deal with the changes from,
92 for example, ocean acidification? Three notable existing algorithms for pH_T have simplistic and
93 empirical treatments of the effects of ocean acidification. One has no parameterization for OA,
94 but instead provides a suggested time-span for the algorithm (Williams et al. 2016); another uses
95 a simple density interpolation of empirically-derived global changes that, for example, does not
96 distinguish the rapidly changing intermediate North Atlantic from the comparatively-static
97 intermediate subpolar North Pacific (Carter et al. 2018); and the one last uses a regional
98 empirical approach that risks mis-attributing long term change and natural variability in pH_T
99 (Bittig et al. 2018). Broullón et al. (2020) also use an empirical relationship to capture the
100 effects of OA for their DIC algorithm. These algorithms are expected to become increasingly
101 biased under future OA conditions.

102 In this paper we improve upon existing algorithms with new methods and new observational data
103 products and encode them into a package of software routines in the MATLAB language. We
104 also introduce a new neural-network approach that can return estimates from more diverse
105 combinations of predictors than previous efforts. We also improve how the algorithms handle
106 C_{ant} impacts on DIC and pH_T , and the new approach should allow future projections of these
107 properties to be useful over longer time horizons while avoiding bias from empirical fits to
108 interannual variability.

109 **2. Methods**

110 *2.1 Basics, updates, new methods, and new features*

111 The first of two products in this effort is an improvement upon the Locally-Interpolated
112 Regression (LIR) strategy for global and full-water column seawater alkalinity estimation that
113 was implemented by Carter et al. (2016) and is similar to a method described by Velo et al.
114 (2013). This approach was later updated and extended to estimating seawater pH_T and nitrate
115 (Carter et al., 2018: LIRv2) and was most recently expanded to oxygen, phosphate, and silicate
116 estimates (Carter et al. 2021). The new improvements in LIR-based empirical seawater property
117 estimation routines (called here: `ESPER_LIR`, equivalent to LIRv3), relative to LIRv2, include:

118 1. use of the 2020 release of the GLObal Data Analysis Project data product
119 (GLODAPv2.2020: Olsen et al. 2020), for predictor variables with many thousands of
120 new measurements, particularly in the North Pacific, relative to the GLODAPv2 version
121 used for earlier versions of the global algorithms;
122 2. numerous additional data sets from the Gulf of Mexico and the Mediterranean Sea as
123 training data, fixing large and important data gaps in LIRv2;
124 3. the ability to return estimates of DIC;
125 4. simple and improved estimation of anthropogenic perturbations to pH_T and DIC based on
126 first principles, allowing better predictions of future changes in seawater carbonate
127 chemistry;
128 5. implementation of a distance weighting for the fit in ESPER_LIR, allowing more data to
129 be used for each of the many regressions;
130 6. and ease-of-use changes that allow the insights from the LIR routines to be more easily
131 adapted for regional applications.

132 In addition to LIR updates, we introduce new neural-network-based routines (ESPER_NN) to
133 take advantage of the strengths of neural networks including the ability to model non-linear
134 relationships between predictors and estimated quantities (Tu 1996). In several important ways
135 this new algorithm imitates the design of the “Carbonate system and Nutrients concentration
136 from hYdrological properties and Oxygen using a Neural-network version B” (CANYON)
137 algorithms designed by Sauzède et al. (2017) and updated by Bittig et al. (2018). The significant
138 differences between ESPER_NN and the existing algorithms are:

139 1. inclusion of new data from the GLODAPv2.2020 data product (as with the LIR updates).
140 2. Like ESPER_LIR, ESPER_NN uses a new first-principles-based approach to estimate the
141 impacts of long-term trends for pH_T and DIC.
142 3. ESPER_NN can function with 16 combinations of seawater properties requiring at
143 minimum salinity and coordinate information, while alternative neural network
144 approaches also require oxygen and temperature. While the temperature, salinity, and
145 oxygen are often available and are frequently an ideal predictor combination, there
146 remain applications where oxygen measurements are not available (due to absent, failed,
147 or fouled sensors) or not desired as predictors (such as when estimating preformed
148 properties from only conservative seawater properties, e.g., Carter et al. 2021).

149 By most validation metrics the ESPER_NN routines perform comparably to ESPER_LIR
150 routines and, in some places, they perform better (see: section 3. Assessment). Nevertheless, we
151 contend there are reasons to maintain both approaches. First, the LIR routines offer a degree of
152 simplicity and estimate explicability that lends them additional value. To highlight the
153 explicability of the LIR estimates, we have added the ability to return the coefficients of the
154 equations that were used to produce each estimate as an additional optional routine output. This
155 may be useful when querying the LIR routines for an equation that could be used for a regional
156 study in another application. Similarly, regional coefficients could be added into the

157 ESPER_LIR coefficient files to produce a modified routine that seamlessly transitions to using
158 regional relationships within a specific area such as a marginal sea, while still using the
159 relationships derived for the open ocean outside of that region. Also, as we discuss later, there is
160 merit to having and using multiple routines when the errors in the estimates appear to be partially
161 independent, as appears to be the case with ESPER_LIR and ESPER_NN.

162 Both new routines are freely available as MATLAB functions at Zenodo (Carter 2021) and
163 updates will be made available at the GitHub repository (see: Section 8). Several changes have
164 been made to the LIR function behavior that are noted alongside the reasoning behind the
165 changes in Supplementary Materials S2: Readme.

166 *2.2 Data products, training data, and test data*

167 The primary data product used to train these algorithms is the GLODAPv2.2020 data product
168 update (Olsen et al. 2020). In addition, we added data sets that will be included in the CARbon,
169 tracer and ancillary data In the MEDiterranean Sea (CARIMED) and that are included in the
170 Coastal Ocean Data Analysis Project for North America (CODAP-NA; Jiang et al. 2021) data
171 products. These data from the Mediterranean Sea (46 cruises spanning from 1976 to 2018 and
172 covering all the sub-basins in the Mediterranean Sea) and the Gulf of Mexico (3 cruises spanning
173 2007 to 2012) are included to ensure these important regions are well-constrained and the cruise
174 information is provided in Supplementary Materials S1.1. These data products are focused on
175 internal consistency and are inclusive for carbonate system measurements. We do not make a
176 special effort in this study to incorporate high resolution data from profiling sensors (e.g., 1 m
177 oxygen values) or measurements from data products that focus on macronutrients or oxygen, but
178 note that this could be an area of focus for future development.

179 As with previous versions of LIRs, we excluded data from GLODAPv2 that has not had
180 secondary quality control checks (QC), and further omitted several sets of cruises that had large
181 adjustments or appeared to have noisy measurements at depth (detailed in Supplementary
182 Materials S1: Data). We also excluded measurements from any bottle that lacked measurements
183 for temperature, salinity, oxygen, and macronutrients (phosphate, silicate, and nitrate).

184 Homogenization of the variety of pH measurement types and calculations in GLODAPv2.2020
185 remains a challenge (see: Supplementary Materials S1.2). As with LIRv2, the ESPERs return in
186 situ pH_T estimates that are intended to be consistent by default with pH_T measured
187 spectrophotometrically with purified m-cresol purple indicator dye and converted to in situ
188 conditions, but can be made to return values that are intended to be consistent with pH_T
189 calculated from DIC and TA at in situ conditions (as CANYON-B does by default) using an
190 optional flag. These approaches for arriving at pH_T values have a documented disagreement
191 (Carter et al. 2013, 2018; Williams et al. 2017; Fong and Dickson 2019; Álvarez et al. 2020), and
192 we rely on the relationships developed by Carter et al. (2018) to interconvert between these pH_T
193 estimates. New observations are challenging the assumptions inherent to this approach

194 (Takeshita et al. 2021), but currently there is insufficient data or mechanistic understanding to
195 refine the relationships we use for interconversion.

196 For assessment purposes we must separate validation data from training data and withhold the
197 validation data from the versions of the algorithms used for assessment. It is better to withhold
198 data from entire cruises to avoid obtaining unrealistically high skill estimates when
199 reconstructing data from a synoptic cruise based on algorithms trained with other data from the
200 same cruise. In past versions of LIRs, this assessment was conducted by creating algorithms that
201 iteratively omitted each cruise while reconstructing data from the omitted cruises. However, this
202 strategy would be too computationally intensive to employ with the ESPER_NN and would not
203 provide a clear comparison to the CANYON-B neural network, which was trained with the
204 original GLODAPv2 release. Instead, all data in GLODAPv2.2020 that were added following
205 the original GLODAPv2 release (i.e., all cruises with GLODAPv2 cruise numbers ≥ 1000 and
206 those incorporated from the Gulf of Mexico and the Mediterranean Sea) are used as test data for
207 the validation versions of the algorithms that were trained only with the data in the original
208 GLODAPv2 release. For general use, a release version of the ESPER_LIR and ESPER_NN
209 algorithms were trained with the total data set to benefit from the recent data, and this release
210 version is the only version provided at Zenodo. Data within several marginal seas (the Gulf of
211 Mexico, the Sea of Japan/East Sea, and the Mediterranean Sea) are omitted from the bulk global
212 open-ocean assessment statistics because these are regions where the validation versions of the
213 algorithms have insufficient training data (i.e., none) to produce estimates. Similarly, data from
214 the Arctic (here: north of 67.5°N) are withheld from the global assessment step because the
215 Arctic is a problematic region for algorithms (see Sect. 3.6). Instead, algorithm performance is
216 separately assessed in these regions to explore the limitations of the approaches used (Section
217 3.6). The numbers of valid, quality-controlled measurements available for each algorithm
218 version in each subset of the data are given in Table 1.

219 *2.3 Anthropogenic impacts on carbonate chemistry*

220 The LIPHR (i.e., LIRv2 for pH_T) and CANYON-B algorithms use “estimate year” (i.e., for
221 LIPHR this is the calendar year expressed as a decimal, where the midpoint of the year 2020
222 would be given as 2020.5) as a predictor for seawater properties (or their reconstruction errors in
223 the case of LIPHRv2) to capture the impacts of long-term trends on pH_T estimates and the
224 training data. However, recent research suggests that decadal variability in seawater property
225 trends can rival, regionally, the magnitudes of the secular trends. This is true even for C_{ant} which
226 exhibits a large secular trend (Woosley et al. 2016; DeVries et al. 2017; Carter et al. 2019a).
227 This finding implies that empirical fits risk projecting trends from cyclical natural variability into
228 the future. LIPHR avoids some biases from regional natural variability by using global empirical
229 fits over density intervals, but, as a result, the routine is unable to distinguish between regions
230 with rapid (e.g., the North Atlantic) versus slow (e.g., the North Pacific) C_{ant} accumulation. In
231 addition, LIPHR assumes a fixed OA rate over time, but OA rates might be expected to
232 accelerate due to the approximately exponential increase in atmospheric CO_2 . Therefore, while

233 algorithms like LIPHR seem to accurately predict contemporaneous deep pH_T, it is likely that
234 biases will emerge over the coming years, particularly in regions where C_{ant} penetration is large
235 such as the North Atlantic (Gruber et al. 2019). The risks of natural variability biasing empirical
236 trend projections are perhaps more acute for the properties that have weaker secular trends than
237 DIC and pH_T, such as nutrients and oxygen, although the empirical trends in these properties are
238 usually smaller components of the overall variability in their estimates.

239 Given the challenges associated with accurately quantifying secular changes with short-term,
240 empirical information, ESPER_LIR and _NN rely on a first-principles-based estimate of C_{ant} and
241 its impacts on pH_T. This approach assumes that exponential increases in atmospheric
242 anthropogenic CO₂ should eventually result in marine C_{ant} concentrations that increase at rates
243 proportional to atmospheric anthropogenic CO₂ concentrations. In other words, this approach
244 relies on the assumption that C_{ant} is in transient steady state (Gammon et al. 1982; Tanhua et al.
245 2007); this is an assumption used to adjust data to reference years in the most recent global C_{ant}
246 distribution change estimates for the 1994 to 2007 period (Gruber et al. 2019). This implies that,
247 locally, the ‘shape’ of the C_{ant} vertical profile (or C_{ant} vertical gradient) should remain constant
248 over time while atmospheric CO₂ and ocean C_{ant} values are increasing exponentially according
249 to:

$$250 \quad C_{ant_year_location} = C_{ant_2002_location} e^{0.018989(year-2002)} \quad (1)$$

251 Therefore, if a C_{ant} value is known for a location in a reference year (e.g., C_{ant_2002_location} in
252 2002 c.e.), then C_{ant} can be estimated for that location in a desired year (C_{ant_year_location}). The
253 coefficient within the exponent is derived by solving equation (1) to match Gruber et al. (2019)’s
254 assumption of a ~28% C_{ant} increase over the 13 years from 1994 to 2007 (see: their methods
255 supplement). We note that this approach is not able or intended to resolve non-steady state
256 variations in C_{ant} (Gruber et al. 2019), and the errors in the estimates that result from this
257 deficiency are included implicitly in the assessed overall uncertainty estimates.

258 For the ESPERs, we utilize a gridded C_{ant} product referenced to the year 2002 (Lauvset et al.
259 2016). This product was created using the Transit Time Distribution (TTD) method (Waugh et
260 al. 2006), and gridded to the same 1°x1° latitude/longitude resolution with 33 depth surfaces as
261 the Global Data Analysis Project (GLODAPv2) gridded data product. This reference 2002 field
262 can be used with Eqn. 1 to estimate the difference between C_{ant} in 2002 and C_{ant} in the year in
263 which a measurement was made, or an estimate is desired. Therefore, rather than having a time
264 dependent prediction of pH_T or DIC, we take the following steps to address anthropogenic trends
265 (Fig. 1):

- 266 1. start with the unmodified training data set,
- 267 2. transform all training data to the year 2002 by adding/removing the missing/excess C_{ant} if
268 they are measured before/after 2002,
- 269 3. train the pH_T or DIC algorithms on this modified training data,
- 270 4. predict pH_T or DIC without a time dependence for 2002,

271 5. and transform the C_{ant} to the desired year (if other than 2002), recalculating DIC and pH_{T}
272 with the new C_{ant} total accordingly.

273 Steps 1 through 3 were performed before training the routines, while steps 4 and 5 are performed
274 by the ESPER code each time it is called. Supplementary Materials S1.3 provides more detail
275 for the pH_{T} recalculations noted in step 5.

276 There are uncertainties associated with the assumptions underlying both the 2002 gridded C_{ant}
277 data product and the transient steady state approach—particularly in regions where there are
278 limited measurements of chlorofluorocarbons and other tracers used to calibrate the TTD
279 approach. We therefore assert that Eqn. 1 should not be used to estimate C_{ant} distributions for
280 any application where C_{ant} is of primary interest. However, uncertainties in the adjustments that
281 come from changes in these C_{ant} estimates over time should be modest for a window of time
282 around the year 2002 c.e., the year in which the adjustments are zero by definition. Equation (1)
283 implies that adjustment errors will be smaller than errors in the underlying 2002 C_{ant} distributions
284 for any estimate before 2039 (i.e., the C_{ant} doubling time after 2002). As the training data are
285 also adjusted in step 2, the effective magnitudes of the adjustments are related to the difference
286 between the years of the estimates and the average measurement years of the training data used
287 for those algorithms (which for most regions and algorithms is close to 2002 c.e.). These
288 ESPERs should therefore be used with increasing caution for DIC and pH_{T} after \sim 2030.
289 Regardless of these challenges, this parameterization of OA rates should be more accurate
290 moving forwards than that used by LIPHR, and any improvements in the C_{ant} estimates should
291 directly reduce estimate bias in the modern era and the near future. Notably, implementing this
292 approach decreased overall training data reconstruction root mean squared error for DIC by
293 $>10\%$, and decreased the trend in the DIC reconstruction error from $\sim 0.49 \mu\text{mol kg}^{-1} \text{yr}^{-1}$ to less
294 than $0.03 \mu\text{mol kg}^{-1} \text{yr}^{-1}$. We caution that these assumptions do not explicitly consider declines
295 in ocean carbon uptake efficiency and the assumption of exponential growth can lead to very
296 large DIC accumulations when used for distant projections. Future atmospheric CO_2
297 concentrations are highly uncertain, and user discretion is advised for any projections.

298 There is no time-variance for ESPER estimates of quantities other than pH_{T} and DIC.

299 *2.4 ESPER_LIR construction*

300 ESPER_LIR broadly functions similarly to LIRv2, which is described in detail by Carter et al.
301 (2018). As with LIRv2, the ESPER_LIR algorithms use regression coefficients (C) that are
302 specific to each of 16 equations and 44,957 locations on a 5° latitude \times 5° longitude \times 33 depth
303 ocean interior grid subsampled from the World Ocean Atlas gridded product grid. These
304 coefficients are interpolated in 3D space to the locations where regression coefficients are
305 desired. The algorithm then uses the coefficients with user-provided seawater property predictor
306 information (P) to produce property estimates.

307 The LIR algorithms are constructed by fitting 16 different regressions that relate the properties of
308 interest, X (silicate, nitrate, phosphate, oxygen, TA, DIC, and pH_T), to combinations of up to 5
309 predictor properties, P (including: salinity, potential temperature, nitrate, phosphate, oxygen, and
310 silicate), which are specific to each property of interest (Table 2). Each equation uses between 1
311 and 5 predictor properties and the generalized predictor equation is:

312
$$X = C_0 + \sum_{i=1}^n C_i P_i \quad (2)$$

313 Unlike LIRv2, depth is never used as a predictor for ESPER_LIR and is only used as a
314 coordinate for regression coefficient interpolation. Versions with depth included as a predictor
315 performed similarly or worse than versions with depth omitted during early testing.

316 The regression coefficients C_i and C_0 are fit 44,957 times for each of the 7 estimated properties
317 and each of the 16 equations. At each grid location, “local” data are selected from the subset of
318 all data that are within 15° in latitude, $30^\circ/\cos(\text{latitude})$ in longitude, and within either $(100 +$
319 $z/10)$ meters depth or 0.1 kg m^{-3} of the estimated density of seawater at that coordinate location.
320 Here z is the coordinate depth in meters. As with LIRv2, these window dimensions are
321 iteratively doubled when fewer than 100 measurements fall within the windows. These data
322 selection windows are initially twice as wide as the windows used in LIRv2 in all dimensions.
323 Doubling the baseline size of these windows is intended to include more data on average for the
324 regression fits, introduce more modes of oceanographic variability into the fitting data, and
325 thereby reduce multicollinearity. The average absolute values of regression coefficients in
326 ESPER_LIR are only 80% of the average absolute values of the coefficients in LIRv2,
327 suggesting ESPER_LIR is subject to less multicollinearity than LIRv2. However, widening the
328 windows risks making the regressions less appropriate locally, so a weighting term is used that is
329 equal to:

330
$$W = \max \left(5, \left(\frac{10(\Delta z)}{100+z} \right)^2 + (\cos(\text{lat})(\Delta \text{lon}))^2 + 4(\Delta \text{lat})^2 \right)^{-2} \quad (3)$$

331 The weighting term W reduces the cost of regression misfits to data that are distant or at
332 significantly different depths from the regression coordinate location, and the maximum function
333 caps the weights (at a value equivalent to the weight found when 5° latitude away) to ensure the
334 regressions are not overly fit to data very near the coordinate where the denominator approaches
335 0. The Δz term is the difference between the regression coordinate depth (z) and the depth of the
336 measurements. The Δlon is the minimum difference in the measurement and coordinate
337 longitudes when using either the -180° to 180° or 0° to 360° conventions, and Δlat is the
338 difference between the measurement and coordinate latitudes. The regression coefficients
339 (C_0 and C_{Pi}) are then fit using a regression of the form:

340
$$XW = (C_0 + \sum_{i=1}^n C_{Pi} P_i)W \quad (4)$$

341 As with LIRv2, data outside of the Atlantic, Mediterranean, and Arctic are excluded when fitting
342 Northern Hemisphere regression coordinates within the Atlantic, Mediterranean, or Arctic—and

343 vice versa—in order to prevent use of data from across Central America or the Bering Strait.
344 The widths of the data inclusion windows and the coefficients in the weighting function were
345 optimized by selecting the variant of 8 combinations that had the best validation statistics.
346 However, some of the combinations yielded comparable results for some predictors, so this
347 parameter tuning process should not be considered exhaustive.

348 *2.5 ESPER_NN Construction*

349 ESPER_NN relies upon a collection of feed-forward neural-networks to estimate seawater
350 properties with a similar operation to the LIR algorithm and a similar structure to the CANYON-
351 B algorithm: ESPER_NN uses the same combination of predictor measurements as ESPER_LIR
352 to produce estimates of the same properties, and does so with a function call that has similar
353 syntax. Unlike ESPER_LIR, in addition to the predictors noted in Table 2, the ESPER_NN
354 algorithm uses latitude, depth, $\cos(\text{longitude}-20^\circ\text{E})$, and $\cos(\text{longitude}-110^\circ\text{E})$ as predictors in
355 each equation, making the estimates somewhat more analogous to a mapping approach than the
356 ESPER_LIR estimates. Similar, but not identical, parameters are used in CANYON (Sauzède et
357 al. 2017) and CANYON-B (Bittig et al. 2018): unlike the original CANYON, ESPER_NN
358 offsets the 0 longitude for the reasons noted by Bittig et al. (2018), specifically that $\cos(\text{lon})$
359 loses explanatory power at the prime meridian, which is a region of oceanographic significance.
360 Offsetting longitudes to 20°E (and 110°E) puts these regions of minimum explanatory power
361 over land masses to the extent possible.

362 ESPER_NN uses 896 neural networks in total: eight neural networks (four in each of two large
363 ocean regions: see below) are used for each of the 16 combinations of predictors used for each of
364 the 7 property estimates. ESPER_NN averages estimates from a “committee” or ensemble of 4
365 neural networks with different combinations of neurons and hidden layers to minimize the
366 impact of errors from any one neural network. These four neural networks include a single one-
367 hidden-layer network with 40 neurons, and three two-hidden-layer networks with 30/10, 25/15,
368 and 20/20 neurons in the 1st/2nd hidden layers. One committee of neural networks is used in the
369 Indo-Pacific-Southern Ocean regions and an additional committee used in the Atlantic Ocean,
370 Arctic Ocean, and Mediterranean Sea. The ESPER_NN algorithm linearly interpolates between
371 the outputs of these two committees of neural networks by latitude across the Southern Atlantic
372 and the Bering Sea, being fully in the Indo-Pacific-Southern Ocean network by 44°S in the
373 Southern Atlantic and fully in the Atlantic, Arctic, and Mediterranean network by 34°S .
374 Similarly, the North-Pacific-to-Arctic transition occurs between 62.5°N and 70°N along Pacific
375 longitudes. After this meridional blending step, there is a zonal transition implemented in the
376 Southern Atlantic between these blended values and the Indo-Pacific-Southern Ocean network
377 starting at 19°E and being completely transitioned at 27°E .

378 Techniques exist for illuminating the relative importance of predictor variables in machine
379 learning approaches (e.g., Olden and Jackson 2002), but the exact equations used by the
380 ESPER_NN algorithm are nevertheless more opaque and less explainable than the LIR

381 equations. The networks are fit using the MATLAB r2017 Machine Learning Toolbox
 382 “feedforwardnet” and “train” function defaults, which include Levenberg Marquardt
 383 optimization with 15% of input data reserved for assessment during iterative fitting steps.
 384 However, the neural networks have been encoded as functions, so users do not require the
 385 Machine Learning Toolbox to operate ESPER_NN.

386 *2.6 Mixed Estimates*

387 Bittig et al. (2018) showed that linear regression and neural network estimates frequently have
 388 independent error fields. From this observation, they proposed that it might be advantageous to
 389 combine estimates from both approaches. We test this idea and find that it has merits in many
 390 circumstances. We therefore also release a wrapper function “ESPER_Mixed.m” that calls both
 391 routines, ESPER_LIR and ESPER_NN, and averages the estimates. We do not provide a similar
 392 wrapper function for CANYON-B, but we note that our assessment suggests the findings for the
 393 mixed approach could also apply to a mixed version of CANYON-B and ESPER_LIR equation
 394 7. The ESPER_Mixed routine is assessed alongside the other algorithms in Section 3.

395 *2.7 Uncertainty estimation*

396 The routines can return uncertainties for every property estimate, and the uncertainty values vary
 397 with input depth and salinity. These uncertainties are estimated at the 1σ (i.e., 1 standard
 398 uncertainty) level, so we would expect ~95% of new measurements that have been through the
 399 GLODAPv2 QC process to fall within windows of \pm twice the ESPER estimated uncertainties.
 400 The LIRv2 uncertainty estimation strategy for TA (Carter et al. 2018) is slightly modified and
 401 then implemented for all properties estimated by the two ESPERs. As before, this approach
 402 interpolates baseline error estimates (E_{X_Est}) in depth and salinity space. The interpolated values
 403 are based on the root-mean-squared errors (RMSEs) of all predictions from the validation
 404 versions of the routines within bins of salinity and depth. As with LIRv2, ESPER_LIR also
 405 scales these methodological uncertainties using user-provided predictor uncertainty estimates.
 406 The following equation is used when the user provides uncertainties for the predictors
 407 ($E_{P_i_Provided}$) that exceed the default assumed input uncertainties (Table 3).

$$408 E_{X_Output} = \sqrt{E_{X_Est}^2 - \sum_{i=1}^n \left(\frac{\partial X}{\partial P_i} E_{P_i_Default} \right)^2 + \sum_{i=1}^n \left(\frac{\partial X}{\partial P_i} E_{P_i_Provided} \right)^2} \quad (5)$$

409 If the optional $E_{P_i_Provided}$ input is omitted then it is assumed that $E_{P_i_Provided}$ equals $E_{P_Default}$
 410 (Table 3), and the two summed terms in this equation cancel. Here $\frac{\partial X}{\partial P_i}$ is the sensitivity of the
 411 property estimate X to the i th predictor P_i and the E_{P_i} terms are the default and the user-provided
 412 predictor uncertainties. For the ESPER_LIRs, the $\frac{\partial X}{\partial P_i}$ values equal the C_{P_i} terms. For
 413 ESPER_NN calculations, the algorithm determines the sensitivities by iteratively perturbing the
 414 input predictors if and only if the user specifies larger-than-default predictor uncertainties. The
 415 uncertainties in Table 3 are the minimum uncertainties allowed by the calculations because these

416 are the assumed uncertainties in the best open ocean training data available, so these
417 uncertainties reflect one of the upper limits on the quality of estimates achievable with the
418 algorithms regardless of the quality of the predictor measurements. The sole difference from the
419 approach used for LIRv2 TA estimates is that the interpolated uncertainties now include the
420 component of uncertainty that originates from potential errors in the training data. This saves a
421 step in the calculations while providing numerically equivalent results.

422 The uncertainty for an ESPER_Mixed estimate is assessed simplistically as the minimum
423 uncertainty assessed for the two component ESPER_LIR and ESPER_NN estimates (Sect. 3.7).

424 **3 Assessment**

425 Routines are validated using versions of the algorithms trained only with the data that were
426 present in the original GLODAPv2 release (Table 1). This cutoff was chosen to make the
427 validation algorithms for ESPER_LIR and ESPER_NN comparable to the LIRv2 and
428 CANYON-B routines to the degree possible. These “validation” versions of the algorithms are
429 then used to recreate the “validation data set,” or the newly added data in the GLODAPv2.2019
430 and GLODAPv2.2020 updates plus the other cruises from the Mediterranean Sea and the Gulf of
431 Mexico. The reconstruction errors for these new measurements are used to derive error statistics
432 for the five routines that we assess (LIRv2, ESPER_LIR, ESPER_NN, CANYON-B, and
433 ESPER_Mixed). The validation data set is in some ways not ideal, in that it is not evenly
434 distributed globally and there is spatial overlap between the test and the training data sets (Fig.
435 2). An alternate approach to assessing prediction errors involves omitting all training data from
436 regions of the ocean representative of data gaps between cruises, and then estimating the errors
437 within these gaps. This approach has been used previously by Sauzède et al. (2017) and Carter
438 et al. (2018), but was found to generally yield smaller uncertainty estimates in the open ocean
439 than approaches that omit entire cruises (Carter et al. 2018), so we conservatively rely on the
440 cruise-omission assessments. The additional data sets from the Gulf of Mexico and the
441 Mediterranean Sea that were incorporated into this paper were omitted from the global-average
442 validation data set because neither had undergone secondary QC and because a small subset of
443 the Mediterranean Sea data from GLODAPv2 had been previously incorporated into the training
444 data product for some algorithms but not others. New measurements from the Sea of Japan/East
445 Sea, a biogeochemically distinct region where no previous measurements existed in the original
446 GLODAPv2 product, are also omitted from bulk validation statistics. However, validation
447 statistics for these regions are given separately (Sect. 3.6).

448 The reported validation statistics are bias (average reconstruction error), root mean squared error
449 (RMSE), and the number of new measurements used for each assessment (N). The 10th, 50th,
450 and 90th error percentiles were examined as potential additional statistics, but these statistics
451 were within expectations when assuming normally distributed errors with the given RMSE and
452 bias statistics.

453 *3.1 Macronutrients*

454 The routines work well for macronutrients (i.e., phosphate, nitrate, and silicate) when given at
455 least two predictors, reproducing the validation data with low average bias and a RMSE that is
456 comparable to the measurement uncertainties (Tables 4 through 6). Phosphate and nitrate have a
457 strong and well-documented covariance in the ocean (Redfield et al. 1963). This covariance
458 results in low RMSE statistics for the equations relating these properties to one another (e.g.,
459 Eqns. 1 and 2 in Table 2), but reduces the value of adding the other as a predictor when one is
460 already included. This covariance is less strong between silicate and either phosphate or nitrate,
461 and oxygen is comparably useful to the macronutrients when predicting silicate. Unsurprisingly,
462 the equations with more fitting parameters tended to perform better, and the RMSE ranged from
463 being comparable to nominal ~2% measurement uncertainty at best (or $\pm 0.04 \mu\text{mol kg}^{-1}$ for a
464 phosphate measurement of $2 \mu\text{mol kg}^{-1}$, A. Olsen et al., 2016) to 3-4 times worse when only S
465 and coordinate information is used in the prediction. All algorithms assessed perform
466 comparably for the equations using T , S , and oxygen as predictors (i.e., ESPER Eqn. 7), but
467 LIRv2 performs slightly worse for silicate. LIRv2 performs comparably to alternatives for many
468 macronutrient estimates, but alternatives outperform LIRv2 for the equations with the largest
469 RMSE values and fewest predictors (e.g., equations 12 and 16), suggesting that the modifications
470 in ESPER_LIR have resulted in an improvement in the least-accurate estimates. Likely, this is
471 due to the larger number of measurements available for each regression in ESPER_LIR relative
472 to LIRv2. Unlike the ESPER_LIR_validation routine assessed here, the released version of
473 ESPER_LIR benefits from including the newly added data in the recent updates to GLODAP,
474 and is therefore preferred to LIRv2 even when the validation statistics are comparable.

475 *3.2 Oxygen*

476 Validation statistics are reasonable for oxygen though persistently greater than the nominal 1%
477 measurement uncertainty (i.e., $3 \mu\text{mol kg}^{-1}$ for a $300 \mu\text{mol kg}^{-1}$ measurement, Olsen et al. 2016),
478 ranging from 4.5 to $13.2 \mu\text{mol kg}^{-1}$ in the global ocean for ESPER_NN_validation and
479 ESPER_LIR_validation (Table 7). LIRv2 is also comparable, but again shows worse validation
480 statistics for equations with fewer predictors and larger RMSE values. The statistics are
481 markedly better at intermediate depths, and range from 2.7 to $6.0 \mu\text{mol kg}^{-1}$ between 1000 and
482 1500 m depth for ESPER_NN_validation. Below the well-lit surface ocean there is no gas
483 exchange and essentially no primary production of organic matter, and the algorithms are
484 therefore better able to capture the fewer processes controlling oxygen distributions. As a result,
485 the oxygen algorithms perform less well at higher oxygen concentrations, which is evident in the
486 larger error statistics globally than in the intermediate depth statistics, as well as in the
487 comparatively diffuse cloud of estimates in the upper right of the oxygen histograms in Fig. 2.
488 Interestingly, the neural network estimates in Fig. 2 appear less diffuse than the LIR-based
489 estimates: the RMSE for eqn. 1 for only the top 200 m is 8.6 , 7.6 , and $8.0 \mu\text{mol kg}^{-1}$ for the LIR,
490 NN, and Mixed validation ESPER variants, respectively. This suggests that the neural network
491 framework is more skillful at capturing the non-linear relationships between properties that can

492 result in the presence of gas exchange and primary production in the surface ocean. Oxygen
493 estimates show a non-negligible bias, overestimating oxygen by an average $0.9 \mu\text{mol kg}^{-1}$ for all
494 3 algorithms across equations. It should be noted that a large amount of the validation data used
495 for this assessment are located within the North Pacific where oxygen concentrations are low, so
496 this could reflect a small regional bias in the algorithms, a tendency to overestimate lower
497 oxygen concentrations, or differences between the test and the training data products.
498 Supporting this idea, the released versions of the algorithms—which use all data as training
499 data—still have a $0.6 \mu\text{mol kg}^{-1}$ bias for the ESPER_Mixed_validation test data reconstructions
500 while having a $-0.1 \mu\text{mol kg}^{-1}$ bias for the ESPER_Mixed_validation training data
501 reconstructions (i.e., GLODAPv2) and no significant bias for both data subsets combined.

502 *3.3 Total Titration Seawater Alkalinity*

503 Seawater alkalinity continues to show strong predictability even with comparatively few
504 predictors (Table 8), and has the smallest relative range in RMSE values with the least precise
505 estimates having a RMSE that is less than double the RMSE of the most precise estimates
506 (ranging from 3.7 to $5.2 \mu\text{mol kg}^{-1}$ for TA for ESPER_NN_validation estimates). The small
507 range in assessed RMSE values is expected because all equations use S , and freshwater cycling is
508 a major driver explaining variability in both S and TA. The excellent validation metrics for new
509 and existing algorithms for TA likely reflect particularly precise TA measurements in the newly
510 added cruises in GLODAPv2.2020, in part due to increased use of certified reference materials
511 for TA (Dickson et al. 2003).

512 Interestingly, there is an estimate bias averaging 0.5 to $1 \mu\text{mol kg}^{-1}$ across equations for the
513 various routines. It is difficult to identify the cause of these average mismatches when
514 considering that the GLODAP secondary QC effort already adjusted several cruises to be in line
515 with the existing GLODAPv2 data product. However, Olsen et al. (2019) note that many of the
516 newly-added cruises in the North Pacific show a negative bias against earlier cruises, consistent
517 with this observation. Also, many of these cruises use single-point spectrophotometric TA
518 titration endpoint detections, which Bockmon & Dickson (2015) previously noted could be a
519 source of disagreement with TA values from full-pH-range titration fits. Interestingly, Sharp &
520 Byrne (2020) have provided a mechanistic explanation that would account for these analytical
521 disagreements if alkaline organic molecules were present in open-ocean seawater. While this
522 discussion highlights the challenges of creating a consistent data product across research groups,
523 the high precision and modest bias of this TA reconstruction nevertheless demonstrates the high
524 quality of the underlying measurements and the importance of the GLODAPv2 secondary QC
525 process.

526 *3.4 In situ pH on the Total Scale*

527 There is some difficulty comparing across pH_T algorithms because the training data for earlier
528 pH_T algorithms were supplemented with several additional cruises (Carter et al. 2018; Bittig et
529 al. 2018), many of which were since added to the GLODAPv2 data product in annual updates.
530 This means that some algorithms would benefit from overlap between the training and validation

531 data products in this comparison. The comparison cannot simply be limited to the truly new
532 cruises because there are not many additional cruises where purified spectrophotometric dye
533 measurements were made that were not used to train earlier algorithms; we limit our comparison
534 to cruises with these spectrophotometric measurements because it has been shown that there are
535 consistent disagreements between measured and calculated pH_T (Carter et al. 2018; Álvarez et al.
536 2020). Moreover, measurements made with purified dyes are consistent with measurements
537 made by sensors that have been shown to have the expected Nernstian response to pH_T changes
538 (Takeshita et al. 2020) lending support to the use of spectrophotometric pH_T values over the
539 disagreeing calculated values. Complicating the comparison further, the three new cruises that
540 were not included in LIRv2 or CANYON-B pH_T training data that do meet our criteria had large
541 adjustments applied during the GLODAP secondary QC. Therefore, for this study we do not re-
542 assess LIRv2 or CANYON-B, and instead show that the ESPERs have similar validation
543 statistics (Table 9) to those published by earlier validation efforts for these algorithms (Carter et
544 al. 2018; Bittig et al. 2018). We do note however, that the statistics obtained when we assess all
545 four algorithms using T , S , and oxygen with the same data (not shown) are quite close to each
546 other despite the partial overlap between training and validation data sets. This suggests all four
547 algorithms are valid for pH_T .

548 It is difficult to read into pH_T validation statistics too much given the comparatively small
549 number of valid assessment data points. However, one pattern in pH_T assessment statistics that
550 is apparent is that pH reconstructions benefit significantly from the use of either nitrate or
551 oxygen as predictors, as these predictors provide information regarding organic matter
552 remineralization. The equations with neither quantity have higher RMSE values, even when
553 silicate is included as a predictor.

554 *3.5 Total Dissolved Inorganic Carbon*

555 The routines reproduce DIC measurements with good skill and a small positive average bias,
556 with RMSE values ranging from 4.8 to 16.7 $\mu\text{mol kg}^{-1}$ globally and 3.2 to 7.0 $\mu\text{mol kg}^{-1}$ at
557 intermediate depths for the various validation versions (Table 10). Assessment statistics are
558 comparable across the three routines that estimate DIC (LIRv2 does not). We caution that DIC
559 does not have seasonal resolution in the surface ocean in most regions of its training data
560 product. Therefore, estimates within the surface ocean should be treated with caution, and we
561 recommend avoiding interpreting seasonality in the ESPER estimates. This caution applies to all
562 property estimates, but is important to note for DIC specifically because of the high sensitivity of
563 DIC to most modes of seasonal variability and the large scientific interest in seasonal DIC
564 cycling. DIC calculations from measured pH or $p\text{CO}_2$ and estimated TA are expected to be less
565 challenged by the lack of seasonal resolution than direct DIC estimates, as TA seasonality is
566 usually less pronounced than DIC seasonality. These two approaches to DIC seasonality
567 reconstruction can return quite different results in the surface ocean (Supplementary Materials
568 S1.4). There are empirical routines for global DIC estimation (Broullón et al. 2020) and surface
569 DIC estimation (Gregor and Gruber 2021) that are also trained with the surface $p\text{CO}_2$

570 measurements. In the many regions where surface $p\text{CO}_2$ has better seasonal data coverage than
571 GLODAPv2, these routines are likely to better resolve DIC surface seasonality than ESPER or
572 other DIC algorithms trained primarily with discrete DIC measurements.

573 *3.6 Regional Tests*

574 We assess the performance of the algorithms in 8 regions independently (Fig. 3). Some of these
575 regions are where biogeochemical Argo floats are currently being deployed (i.e., the North
576 Atlantic, California Current, Equatorial Pacific, and the Southern Ocean) and therefore where
577 there is additional interest in the performance of the algorithms. Other regions are
578 biogeochemically distinct places where there were no training data used for the CANYON-B
579 and/or LIRv2 algorithms (i.e., Sea of Japan/East Sea, Gulf of Mexico, and the Mediterranean).
580 These regions therefore allow tests of the likely errors one can expect when applying global
581 algorithms to biogeochemically distinct regions where there were no available training data.
582 Finally, the Arctic is a problematic region for the algorithms that warrants special attention.

583 We first consider the Southern Ocean, the Equatorial Pacific, the California Current, and the
584 Northern Atlantic. The validation statistics in these regions where there are active ongoing
585 biogeochemical float deployment efforts are, for the most part, consistent with the global average
586 statistics. The Northern Atlantic shows validation statistics that are somewhat worse than global
587 averages for macronutrients and oxygen and the California Current shows oxygen RMSE values
588 that are equally elevated. Given the active physical processes and biogeochemical cycling in
589 these regions of interest (and the comparatively small validation data set in the California
590 Current), none of these sets of validation statistics are unexpected. We therefore conclude that
591 the algorithms should function within expectations in these important regions and suggest Table
592 11 can be used to get a sense for how the global validation statistics might vary on a regional
593 level.

594 The Sea of Japan/East Sea provides an excellent case study to assess the use of algorithms in
595 regions without training data for three reasons: (1) this region had no data in the first
596 GLODAPv2 release, and thus is a region where neither LIRv2 nor CANYON-B had training
597 data; (2) a large quantity of high-quality data from the Sea of Japan/East Sea were included with
598 the GLODAPv2.2020 release; and (3) the Sea of Japan/East Sea is biogeochemically distinct
599 from the open ocean to the east of Japan, providing a challenge for the predictive capabilities of
600 the approaches. Neither of the earlier generation of algorithms work well there with large
601 average biases and RMSE values that are ~9 times greater on average than in the first set of
602 regions considered, but with significant variance between properties and routines (Table 11).
603 LIRv2 is especially problematic in this region, and the marked improvement in
604 ESPER_LIR_validation relative to LIRv2 suggests the wider data inclusion windows did indeed
605 reduce variance inflation in this region. The release versions of the ESPERs that do include data
606 from the Sea of Japan/East Sea as training data indeed reproduce these data with comparable
607 fidelity to the global statistics (Supplementary Materials S1.4). We conclude this region is not a

608 special challenge for algorithms when training data are included. The release versions of these
609 algorithms updated with the new data should therefore work in the now-measured portions of the
610 Sea of Japan/East Sea.

611 Two additional marginal seas deserve mention. GLODAPv2 does not yet include data from the
612 Gulf of Mexico or the Mediterranean Sea that have been subjected to the GLODAPv2 a
613 completed secondary quality control process (some data from the Mediterranean Sea are
614 included, but with QC flags of 0). However, due to the large errors expected within marginal
615 seas (and now demonstrated for the Sea of Japan) when training data are absent or omitted, data
616 from two cruises to the Mediterranean were included in the training data for CANYON-B despite
617 the lack of secondary QC. We now do similarly in the ESPERs and include additional data
618 gathered as part of the CODAP-NA (Jiang et al. 2021) and ongoing CARIMED efforts
619 (Supplementary Materials S1.1). The same lessons from the Sea of Japan/East Sea analysis
620 apply to the reconstruction of measurements from the Gulf of Mexico and the Mediterranean Sea
621 (Table 11). We caution that ESPER_LIR is challenged by the lack of data below 2000 m depth
622 in the Mediterranean, and increases its window sizes large enough to incorporate data at depth
623 from the deep North Atlantic. This results in poor RMSE statistics even when the test data is
624 included with the training data (Supplementary Materials S1.4). Until this is addressed, it is
625 recommended that users interested in this area use ESPER_NN or CANYON_MED (Fourrier et
626 al. 2020) in place of ESPER_LIR or ESPER_Mixed. Such regional algorithms can be
627 meaningfully better for regional efforts, and work in progress on a regional algorithm for the
628 Gulf of Mexico shows promise for reducing the RMS misfit to the observations from this region.
629 The Gulf of Mexico challenges the ESPERs because this is a region where the underlying TTD-
630 based C_{ant} data product does not contain estimates, so C_{ant} is crudely triangulated between the
631 Pacific and Atlantic in this region. A regional algorithm could address this limitation with a
632 more sophisticated approach.

633 Finally, with intense seasonality, strong freshwater cycling and riverine inputs, seasonal ice
634 cover, and broad continental shelves, the Arctic is an interesting “worst case scenario” for the
635 algorithms, even when training data are available. The validation statistics in this region are
636 significantly worse than the global statistics (RMSEs average ~2.3 times greater, though again
637 with variance between properties and routines, Table 11). These larger uncertainties found in the
638 Arctic could perhaps be generalized to other problematic regions such as shallow coastal areas,
639 small marginal seas, areas with significant riverine inputs, or other areas with seasonal ice cover.

640 3.7 Mixed ESPER

641 As proposed by Bittig et al. (2018), averaging the estimates from ESPER_LIR_validation and
642 _NN_validation indeed seems to improve the global average prediction statistics, though the
643 improvement is sometimes small and often the individual residuals are greater with the
644 ESPER_Mixed estimate than for the better of the two estimates. For equations with few
645 predictors (e.g., equation 16, using S as the only seawater property predictor) the improvement in

646 the global open-ocean average RMSE is pronounced for all 7 properties estimated by the
647 routines. We therefore recommend using ESPER_Mixed over ESPER_LIR or ESPER_NN
648 unless there is reason to prefer one approach over another due to, for example, the results of a
649 regional validation exercise in the region of interest.

650 **4. Discussion and summary statements**

651 Several patterns hold across the various properties. For example, including more predictors
652 leads to better estimates on average (Fig. 4, showing an average across all properties for both
653 ESPERs) when the predictor measurements are high quality (i.e., comparable to the
654 measurements in GLODAPv2). However, estimate improvements are marginal beyond 4
655 predictors. Also, equations 6 and 7 do nearly as well as any equation despite having only 3
656 predictors (i.e., temperature; salinity; and either oxygen, nitrate, or phosphate, depending on the
657 predicted property). This observation shows the predictive power of including at least one
658 macronutrient or oxygen as a predictor for biogeochemical properties.

659 A second important generalization is that all predictions do better at depth (>1000 m) though this
660 is especially the case for gas distribution reconstructions: the intermediate-depth RMSE values
661 average 55% of the global RMSE values for oxygen, pH_T, and DIC (Tables 7, 9, and 10,
662 respectively) whereas they average ~70% of the global RMSE values for phosphate, nitrate,
663 silicate, and TA (Tables 4, 5, 6, and 8, respectively). The larger, near surface estimate errors for
664 parameters influenced by air-sea gas exchange (e.g., pH_T, DIC, and oxygen) are likely the result
665 of their decoupling with predictor variables that are not gases (or are gases with different
666 equilibration and residence times). These changes in parameter relationships near the surface
667 due to air-sea exchange are also sensitive to dynamic processes (e.g., wind speed), which are not
668 well captured by the predictor parameters, and are thus difficult to parameterize in static
669 algorithm relationships.

670 Finally, regional errors are sometimes significantly larger than global open-ocean errors, and
671 regional biases are almost always larger than the global biases. This highlights an important
672 caution for users of these routines: the global statistics may not be appropriate for estimates over
673 a more limited area. For this we note both that it is important to validate the algorithm estimates
674 for a given region/application and to consider how large of an average estimate bias is likely for
675 a region of a given size. As an example, we have assessed how the bias decreases as the size of
676 the latitude and longitude window considered increases for ESPER_NN_validation nitrate
677 estimates (Fig. 5). These average regional biases are computed by iteratively averaging all
678 estimate errors inside windows of a given size around each of the grid points used by the LIR
679 routines. Then, for each window size considered we compute an area-weighted average of the
680 absolute values of the bias estimates for the grid points. In the example presented, the average
681 estimate bias is approximately half of the global RMSE when estimates are averaged over a
682 10°x10° window, and as expected the bias becomes smaller as the averaging window grows.
683 This shows that the estimates retain significant regional bias, implying nearby algorithm
684 estimates cannot be treated as statistically independent. For a float or mooring that stays within a

685 small spatial region, this algorithm bias could be somewhat worse still than shown in Fig. 5. For
686 $p\text{CO}_2$ calculations based on pH_T measurements that are adjusted to algorithm values, even a
687 small average bias could lead to a meaningful change in calculated air-sea CO_2 flux.

688 5. Comments and recommendations

689 We have updated global algorithms for seawater biogeochemical property estimation and their
690 associated MATLAB routines with new functionality using new methods and new data. We
691 show that our new methods are mechanistically at least as skillful as earlier methods and are in
692 some cases better. They also have the advantages of being trained with the latest quality-
693 controlled data products, easy to implement in MATLAB, capable of estimating a variety of
694 seawater properties, flexible with the choice of input parameters, and capable of adapting several
695 aspects of their outputs to user needs (e.g., calculated-like or measured-like pH_T). Where
696 possible, our validation statistics provide comparisons using validation versions of the algorithms
697 with identical training and validation data sets for all versions of the routines assessed. We
698 therefore recommend these updates even when validation metrics are comparable to those of
699 earlier routines because the newer routines are trained from a larger data set with better temporal
700 and spatial coverage. Two important features of our new routines are (1) the flexibility to predict
701 many seawater properties from 16 combinations of seawater properties using either a regression
702 approach or a neural network approach and (2) the implementation of a simple estimate of the
703 impacts of C_{ant} on pH_T and DIC based on first principles. While the new C_{ant} estimation strategy
704 is an improvement over the LIRv2 approach for estimating the impacts of OA on pH, it
705 nevertheless is quite simplistic and should not be relied upon when C_{ant} distributions are
706 themselves of interest.

707 We test the practice of averaging estimates from multiple algorithms and find that it frequently
708 improves estimates (in a global open-ocean RMSE sense). This practice is therefore
709 recommended for most applications, and we suggest further improvements might be obtained by
710 averaging estimates from still more algorithms such as CANYON-B or its updates. A wrapper
711 function for averaging CANYON-B values is under development and may eventually be
712 included at the same GitHub repository as the ESPER functions.

713 Our assessment also revealed/reinforced several important ideas to consider when using
714 algorithm estimates: First it is critical to have measurements in the training data set that are near
715 to the region in which estimates are desired. Poor reconstructions of the properties of seawater
716 in the Sea of Japan/East Sea from the versions of the routines that did not include measurements
717 in this Sea highlight the importance of this caution. Writeups of earlier algorithm assessment
718 efforts also cautioned against the use of the algorithms in coastal environments and marginal seas
719 where the algorithms did not have training data, but this case study helps quantify the large likely
720 errors when proceeding despite this caution, as many data-poor marginal seas remain. Second,
721 global oxygen, DIC, and pH estimation routine validation statistics are not as strong as the
722 equivalent statistics when limited to intermediate depths. This is likely because the current

723 generation of algorithms lacks data with sufficient temporal resolution to capture seasonal or
724 shorter patterns of variability associated with gas exchanges. It is possible that the algorithms
725 could be improved by incorporating measurements from the biogeochemical Argo array or other
726 data products that are more seasonally resolved than GLODAPv2, though care would have to be
727 taken to avoid reinforcing the algorithms with float data that is calibrated against earlier versions
728 of the algorithms. This could perhaps be accomplished by removing float measurements that
729 reside below the depths that experience seasonal variability from the data products used to train
730 these future algorithms. At least until such an improvement is made seasonal variability in the
731 estimated fields should be treated with caution.

732 At intermediate depths, ESPER_LIR_validation equation 8 reproduces oxygen with an RMSE of
733 4.8 $\mu\text{mol kg}^{-1}$ using only T and S as predictors (and 3.7 $\mu\text{mol kg}^{-1}$ for
734 ESPER_Mixed_validation), raising the possibility that estimates could be used to check oxygen
735 sensor performance on in situ platforms. Currently, most float oxygen sensors are subjected to a
736 1-point gain calibration against air-oxygen readings or climatological values at high oxygen
737 concentrations, and a deep algorithm estimate could allow a 2-point check that would assess
738 sensor performance at low oxygen saturation. Comparisons at park depths could circumvent
739 potential issues associated with slow sensor response times.

740 Our use of a smaller committee of neural networks with somewhat fewer nodes/neurons than is
741 used by CANYON-B is a pragmatic decision based on the computational costs associated with
742 training neural networks for many combinations of predictors and regions, and we have only
743 done a small amount of neural network structure optimization. However, it should be noted that
744 our use of separate network committees for the Indo-Pacific and Arctic-Atlantic regions
745 effectively doubles the complexity of our networks, and that increasing the complexity further
746 did not seem to meaningfully improve our predictions in limited trials. It is nevertheless likely
747 that further improvements in fit and predictive power could be obtained with additional tuning.

748 While the neural networks are powerful, we demonstrate that the regression-based approach of
749 the ESPER_LIR routines can nevertheless yield comparably skillful estimates in the open ocean
750 or under the right conditions. We contend that the LIR machinery has an advantage of being
751 more explainable than a neural network, and therefore that the LIRs serve a valuable role among
752 seawater prediction routines. An example of where that could prove useful would be in adapting
753 the LIRs to work in an inland sea. A user could append their own grid of regression coefficients
754 determined for a marginal sea such as the Baltic or Mediterranean Seas or an inland waterway
755 such as the Puget Sound, and the routine would transition seamlessly between global estimates
756 and regionally appropriate estimates. This is a future direction for LIR development that would
757 require partnerships with researchers investigating such bodies of water.

758 The ESPER_LIR routine lacks predictors derived from coordinate information—rather, this
759 information is used in the interpolation of regression coefficients only. As a result, the LIR
760 routines struggle more than the neural networks when applied in regions that are dissimilar from

761 the training data in property space but are nearby in physical space. This can be seen clearly as
762 larger reconstruction errors in the Mediterranean, the Gulf of Mexico, and the Sea of Japan/East
763 Sea. This was doubly true for the LIRv2 routines which tended to also be less well-constrained
764 than the ESPER_LIR (i.e., LIRv3) routines. By contrast, the neural networks also struggle, but
765 tend to have better RMSE statistics for these regions. We reiterate that the release versions of
766 the ESPERs should substantially outperform the bleak assessment statistics given for such
767 regions because the release versions of these routines are trained with data in these regions
768 (unlike the _validation versions, which are used to highlight the dangers of using algorithms in
769 regions where they were not trained).

770 **6. Acknowledgements**

771 Carter, Feely, and Wanninkhof thank the Global Ocean Monitoring and Observing (GOMO)
772 program of the National Oceanic and Atmospheric Administration (NOAA) for funding
773 algorithm development under the Carbon Data Management and Synthesis Grant (Fund ref.
774 #100007298). Regional data contributions and validation efforts originate from NOAA National
775 Oceanographic Partnership Program (NOPP) funding (NA19OAR4310362), the NOAA Ocean
776 Acidification Program, and GOMO support for biogeochemical Argo. We further thank the
777 scientists and crew aboard the research vessels that collected these data, and the National Science
778 Foundation and the NOAA GOMO program for supporting the critical Global Ocean Ship-based
779 Hydrographic Investigations Program and other cruise programs. Bittig acknowledges funding
780 from the DArgo2025 project (grant No. 03F0857D). Fassbender was supported by GOMO.
781 Álvarez was supported by the RADIALES, RADPROF and MedSHIP IEO monitoring
782 programs. This research was carried out in part under the auspices of the Cooperative Institutes
783 for Climate, Ocean, and Ecosystem Studies (CICOES) and Marine and Atmospheric Studies
784 (CIMAS), Cooperative Institutes between Universities of Washington and Miami (respectively)
785 and the National Oceanic and Atmospheric Administration, cooperative agreement #s
786 NA15OAR4320063 and NA20OAR4320472, respectively. This is CICOES contribution
787 number 2020-1138 and PMEL contribution number 5243.

788 **7. Data availability**

789 The training data are available from the GLODAPv2.2020 data product
790 (<https://www.gladap.info/>). The data from the Gulf of Mexico are available from the National
791 Center for Environmental Information (https://www.ncei.noaa.gov/access/ocean-carbon-data-system/oceans/Coastal/NACP_East.html). The training data from the Mediterranean are
792 compiled as part of the ongoing CARIMED data product synthesis that will be made public
793 through the GLODAP information page. These cruises are listed in Supplementary Materials
794 S1.1 and can be obtained online individually from the National Center for Environmental
795 Information (e.g., <https://www.ncei.noaa.gov/access/metadata/landing-page/bin/iso?id=gov.noaa.nodc:0214546>) or, for some cruises, the Pangaea webpage
796 (<https://www.pangaea.de/>).

799 **8. Code Availability**
800 The algorithms are publicly accessible and archived as submitted at Zenodo (Carter 2021)
801 <https://doi.org/10.5281/zenodo.5348388>, and updates will be maintained at the GitHub
802 repository <https://github.com/BRCSscienceProducts/ESPER>.

803 **9. Competing Interests**
804 The authors declare that they have no conflict of interest.

805 **10. Author contributions**
806 Carter led the data compilation, coding, figure generation, and writing efforts. Bittig,
807 Fassbender, Sharp, Takeshita, and Xu provided guidance and input on the code structure and
808 format and aided with testing the routines and iterating on them and their documentation.
809 Fassbender generated several key figures. Alvarez, Barbero, and Fassbender identified and
810 provided key data sets. Wanninkhof and Feely played significant roles in securing and sustaining
811 funding for this effort. Critically, all authors aided with writing and vetting this manuscript and
812 provided comments and feedback at multiple stages during planning and writing.

813 **11. References**

814

815 Álvarez, M., N. M. Fajar, B. R. Carter, E. F. Guallart, F. F. Pérez, R. J. Woosley, and A. Murata.
816 2020. Global Ocean Spectrophotometric pH Assessment: Consistent Inconsistencies.
817 *Environ. Sci. Technol.* **54**: 10977–10988. doi:10.1021/acs.est.9b06932

818 Bittig, H. C., T. Steinhoff, H. Claustre, B. Fiedler, N. L. Williams, R. Sauzède, A. Körtzinger,
819 and J.-P. Gattuso. 2018. An Alternative to Static Climatologies: Robust Estimation of Open
820 Ocean CO₂ Variables and Nutrient Concentrations From T, S, and O₂ Data Using Bayesian
821 Neural Networks. *Front. Mar. Sci.* **5**: 328. doi:10.3389/fmars.2018.00328

822 Bockmon, E. E., and A. G. Dickson. 2015. An inter-laboratory comparison assessing the quality
823 of seawater carbon dioxide measurements. *Mar. Chem.* **171**: 36–43.
824 doi:10.1016/J.MARCHEM.2015.02.002

825 Broullón, D., F. F. Pérez, A. Velo, and others. 2019. A global monthly climatology of total
826 alkalinity: A neural network approach. *Earth Syst. Sci. Data* **11**: 1109–1127.
827 doi:10.5194/essd-11-1109-2019

828 Broullón, D., F. F. Pérez, A. Velo, and others. 2020. A global monthly climatology of oceanic
829 total dissolved inorganic carbon: A neural network approach. *Earth Syst. Sci. Data* **12**:
830 1725–1743. doi:10.5194/essd-12-1725-2020

831 Bushinsky, S. M., Y. Takeshita, and N. L. Williams. 2019. Observing Changes in Ocean
832 Carbonate Chemistry: Our Autonomous Future. *Curr. Clim. Chang. Reports* **5**: 207–220.
833 doi:10.1007/s40641-019-00129-8

834 Carter, B. R. 2021. Empirical Seawater Property Estimation Routines,
835 revisions. doi:10.5281/ZENODO.5348388

836 Carter, B. R., R. A. Feely, S. K. Lauvset, A. Olsen, T. DeVries, and R. Sonnerup. 2021.
837 Preformed Properties for Marine Organic Matter and Carbonate Mineral Cycling
838 Quantification. *Global Biogeochem. Cycles* **35**: e2020GB006623.
839 doi:10.1029/2020GB006623

840 Carter, B. R., R. A. Feely, S. Mecking, and others. 2017. Two decades of Pacific anthropogenic

841 carbon storage and ocean acidification along Global Ocean Ship-based Hydrographic
842 Investigations Program sections P16 and P02. *Global Biogeochem. Cycles* **31**: 306–327.
843 doi:10.1002/2016GB005485

844 Carter, B. R., R. A. Feely, R. Wanninkhof, and others. 2019a. Pacific Anthropogenic Carbon
845 Between 1991 and 2017. *Global Biogeochem. Cycles* 2018GB006154.
846 doi:10.1029/2018GB006154

847 Carter, B. R., R. A. Feely, N. L. Williams, A. G. Dickson, M. B. Fong, and Y. Takeshita. 2018.
848 Updated methods for global locally interpolated estimation of alkalinity, pH, and nitrate.
849 *Limnol. Oceanogr. Methods* **16**: 119–131. doi:10.1002/lom3.10232

850 Carter, B. R., J. A. Radich, H. L. Doyle, and A. G. Dickson. 2013. An automated system for
851 spectrophotometric seawater pH measurements. *Limnol. Oceanogr. Methods* **11**: 16–27.
852 doi:10.4319/lom.2013.11.16

853 Carter, B. R., N. L. Williams, W. Evans, A. J. Fassbender, L. Barbero, C. Hauri, R. A. Feely, and
854 A. J. Sutton. 2019b. Time of Detection as a Metric for Prioritizing Between Climate
855 Observation Quality, Frequency, and Duration. *Geophys. Res. Lett.* **46**: 3853–3861.
856 doi:10.1029/2018GL080773

857 Carter, B. R., N. L. Williams, A. R. Gray, and R. A. Feely. 2016. Locally interpolated alkalinity
858 regression for global alkalinity estimation. *Limnol. Oceanogr. Methods* **14**: 268–277.
859 doi:10.1002/lom3.10087

860 DeVries, T., M. Holzer, and F. Primeau. 2017. Recent increase in oceanic carbon uptake driven
861 by weaker upper-ocean overturning. *Nature* **542**: 215–218. doi:10.1038/nature21068

862 Dickson, A. G., J. D. Afghan, and G. C. Anderson. 2003. Reference materials for oceanic CO₂
863 analysis: a method for the certification of total alkalinity. *Mar. Chem.* **80**: 185–197.
864 doi:10.1016/S0304-4203(02)00133-0

865 Doney, S. C., D. S. Busch, S. R. Cooley, and K. J. Kroeker. 2020. The impacts of ocean
866 acidification on marine ecosystems and reliant human communities. *Annu. Rev. Environ.*
867 *Resour.* **45**: 83–112. doi:10.1146/annurev-environ-012320-083019

868 Doney, S. C., V. J. Fabry, R. A. Feely, and J. A. Kleypas. 2009. Ocean acidification: the other
869 CO₂ problem. *Ann. Rev. Mar. Sci.* **1**: 169–192. doi:10.1146/annurev.marine.010908.163834

870 Durack, P. J., S. E. Wijffels, and R. J. Matear. 2012. Ocean salinities reveal strong global water
871 cycle intensification during 1950 to 2000. *Science* **336**: 455–8.
872 doi:10.1126/science.1212222

873 Feely, R. A., S. Doney, and S. Cooley. 2009. Ocean Acidification: Present Conditions and Future
874 Changes in a High-CO₂ World. *Oceanography* **22**: 36–47. doi:10.5670/oceanog.2009.95

875 Feely, R. A., C. L. Sabine, K. Lee, W. Berelson, J. Kleypas, V. J. Fabry, and F. J. Millero. 2004.
876 Impact of anthropogenic CO₂ on the CaCO₃ system in the oceans. *Science* **305**: 362–6.
877 doi:10.1126/science.1097329

878 Fong, M. B., and A. G. Dickson. 2019. Insights from GO-SHIP hydrography data into the
879 thermodynamic consistency of CO₂ system measurements in seawater. *Mar. Chem.* **211**:
880 52–63.

881 Fourrier, M., L. Coppola, H. Claustre, Fabrizio D'Ortenzio, R. Sauzède, and J.-P. Gattuso. 2020.
882 A Regional Neural Network Approach to Estimate Water-Column Nutrient Concentrations
883 and Carbonate System Variables in the Mediterranean Sea: CANYON-MED. *Front. Mar.*
884 *Sci.* **7**: 1–20. doi:10.3389/fmars.2020.00620

885 Gammon, R. H., J. Cline, and D. Wisegarver. 1982. Chlorofluoromethanes in the northeast
886 Pacific Ocean: Measured vertical distributions and application as transient tracers of upper

887 ocean mixing. *J. Geophys. Res.* **87**: 9441. doi:10.1029/JC087iC12p09441

888 Gattuso, J.-P., A. Magnan, R. Bille, and others. 2015. Contrasting futures for ocean and society
889 from different anthropogenic CO₂ emissions scenarios. *Science* (80-). **349**.
890 doi:10.1126/science.aac4722

891 Goyet, C., R. Healy, J. Ryan, and A. Kozyr. 2000. Global Distribution of Total Inorganic Carbon
892 and Total Alkalinity below the Deepest Winter Mixed Layer Depths.

893 Gray, A. R., K. S. Johnson, S. M. Bushinsky, and others. 2018. Autonomous Biogeochemical
894 Floats Detect Significant Carbon Dioxide Outgassing in the High-Latitude Southern Ocean.
895 *Geophys. Res. Lett.* **45**: 9049–9057. doi:10.1029/2018GL078013

896 Gregor, L., and N. Gruber. 2021. OceanSODA-ETHZ: a global gridded data set of the surface
897 ocean carbonate system for seasonal to decadal studies of ocean acidification. *Earth Syst.*
898 *Sci. Data* **13**: 777–808. doi:10.5194/essd-13-777-2021

899 Gruber, N., D. Clement, B. R. Carter, and others. 2019. The oceanic sink for anthropogenic CO₂
900 from 1994 to 2007. *Science* (80-). **363**: 1193–1199. doi:10.1126/science.aau5153

901 van Heuven, S., D. Pierrot, J. W. B. Rae, E. Lewis, and D. W. R. Wallace. 2011. MATLAB
902 program developed for CO₂ system calculations, CO2sys.

903 Jiang, L.-Q., B. R. Carter, R. A. Feely, S. K. Lauvset, and A. Olsen. 2019. Surface ocean pH and
904 buffer capacity: past, present and future. *Sci. Rep.* **9**: 18624. doi:10.1038/s41598-019-
905 55039-4

906 Jiang, L. Q., R. A. Feely, R. Wanninkhof, and others. 2021. Coastal Ocean Data Analysis
907 Product in North America (CODAP-NA)-an internally consistent data product for discrete
908 inorganic carbon, oxygen, and nutrients on the North American ocean margins. *Earth Syst.*
909 *Sci. Data* **13**: 2777–2799. doi:10.5194/ESSD-13-2777-2021

910 Johnson, K. S., J. N. Plant, L. J. Coletti, and others. 2017. Biogeochemical sensor performance in
911 the SOCCOM profiling float array.,

912 Khatiwala, S., T. Tanhua, S. Mikaloff Fletcher, and others. 2013. Global ocean storage of
913 anthropogenic carbon. *Biogeosciences* **10**: 2169–2191. doi:10.5194/bg-10-2169-2013

914 Landschützer, P., T. Ilyina, and N. S. Lovenduski. 2019. Detecting Regional Modes of
915 Variability in Observation-Based Surface Ocean pCO₂. *Geophys. Res. Lett.* **46**.
916 doi:10.1029/2018GL081756

917 Lauvset, S. K., R. M. Key, A. Olsen, and others. 2016. A new global interior ocean mapped
918 climatology: the 1° × 1° GLODAP version 2. *Earth Syst. Sci. Data* **8**: 325–340.
919 doi:10.5194/ESSD-8-325-2016

920 Lee, K., L. T. Tong, F. J. Millero, and others. 2006. Global relationships of total alkalinity with
921 salinity and temperature in surface waters of the world's oceans. *Geophys. Res. Lett.* **33**:
922 L19605. doi:10.1029/2006GL027207

923 Nerem, R. S., B. D. Beckley, J. T. Fasullo, B. D. Hamlington, D. Masters, and G. T. Mitchum.
924 2018. Climate-change–driven accelerated sea-level rise detected in the altimeter era. *Proc.*
925 *Natl. Acad. Sci. U. S. A.* **115**: 2022–2025. doi:10.1073/pnas.1717312115

926 Olden, J. D., and D. A. Jackson. 2002. Illuminating the “black box”: A randomization approach
927 for understanding variable contributions in artificial neural networks. *Ecol. Modell.* **154**:
928 135–150. doi:10.1016/S0304-3800(02)00064-9

929 Olsen, A., R. M. Key, S. van Heuven, and others. 2016. The Global Ocean Data Analysis Project
930 version 2 (GLODAPv2) – an internally consistent data product for the world ocean. *Earth*
931 *Syst. Sci. Data* **8**: 297–323. doi:10.5194/essd-8-297-2016

932 Olsen, A., N. Lange, R. M. Key, and others. 2019. GLODAPv2.2019 - An update of

933 GLODAPv2. *Earth Syst. Sci. Data* **11**. doi:10.5194/essd-11-1437-2019

934 Olsen, A., N. Lange, R. M. Key, and others. 2020. An updated version of the global interior
935 ocean biogeochemical data product, GLODAPv2.2020. *Earth Syst. Sci. Data* **12**: 3653–
936 3678. doi:10.5194/essd-12-3653-2020

937 Purkey, S. G., and G. C. Johnson. 2013. Antarctic Bottom Water Warming and Freshening:
938 Contributions to Sea Level Rise, Ocean Freshwater Budgets, and Global Heat Gain. *J. Clim.*
939 **26**: 6105–6122. doi:10.1175/JCLI-D-12-00834.1

940 Redfield, A. C., B. H. Ketchum, and A. F. Richards. 1963. The influence of organisms on the
941 composition of seawater. *Sea* **2**: 26–77.

942 Roemmich, D., W. John Gould, and J. Gilson. 2012. 135 years of global ocean warming between
943 the Challenger expedition and the Argo Programme. *Nat. Clim. Chang.* **2**: 425–428.
944 doi:10.1038/nclimate1461

945 Sabine, C. L., R. A. Feely, N. Gruber, and others. 2004. The oceanic sink for anthropogenic CO₂.
946 *Science* **305**: 367–71. doi:10.1126/science.1097403

947 Sasano, D., Y. Takatani, N. Kosugi, T. Nakano, T. Midorikawa, and M. Ishii. 2018. Decline and
948 Bidecadal Oscillations of Dissolved Oxygen in the Oyashio Region and Their Propagation
949 to the Western North Pacific. *Global Biogeochem. Cycles* **32**: 909–931.
950 doi:10.1029/2017GB005876

951 Sauzède, R., H. C. Bittig, H. Claustre, O. Pasqueron de Fommervault, J.-P. Gattuso, L. Legendre,
952 and K. S. Johnson. 2017. Estimates of Water-Column Nutrient Concentrations and
953 Carbonate System Parameters in the Global Ocean: A Novel Approach Based on Neural
954 Networks. *Front. Mar. Sci.* **4**: 128. doi:10.3389/fmars.2017.00128

955 Sharp, J. D., and R. H. Byrne. 2020. Interpreting measurements of total alkalinity in marine and
956 estuarine waters in the presence of proton-binding organic matter. *Deep. Res. Part I
957 Oceanogr. Res. Pap.* **165**: 103338. doi:10.1016/j.dsr.2020.103338

958 Takeshita, Y., K. S. Johnson, L. J. Coletti, H. W. Jannasch, P. M. Walz, and J. K. Warren. 2020.
959 Assessment of pH dependent errors in spectrophotometric pH measurements of seawater.
960 *Mar. Chem.* **223**: 103801. doi:10.1016/j.marchem.2020.103801

961 Takeshita, Y., K. S. Johnson, T. R. Martz, J. N. Plant, and J. L. Sarmiento. 2018. Assessment of
962 Autonomous pH Measurements for Determining Surface Seawater Partial Pressure of CO₂.
963 *J. Geophys. Res. Ocean.* **123**. doi:10.1029/2017JC013387

964 Takeshita, Y., J. K. Warren, X. Liu, and others. 2021. Consistency and stability of purified meta-
965 cresol purple for spectrophotometric pH measurements in seawater. *Mar. Chem.* **236**:
966 104018. doi:10.1016/J.MARCHEM.2021.104018

967 Tanhua, T., A. Körtzinger, K. Friis, D. W. Waugh, and D. W. R. Wallace. 2007. An estimate of
968 anthropogenic CO₂ inventory from decadal changes in oceanic carbon content. *Proc. Natl.
969 Acad. Sci. U. S. A.* **104**: 3037–42. doi:10.1073/pnas.0606574104

970 Tu, J. V. 1996. Advantages and disadvantages of using artificial neural networks versus logistic
971 regression for predicting medical outcomes. *J. Clin. Epidemiol.* **49**: 1225–1231.
972 doi:10.1016/S0895-4356(96)00002-9

973 Velo, A., F. F. Pérez, T. Tanhua, M. Gilcoto, A. F. Ríos, and R. M. Key. 2013. Total alkalinity
974 estimation using MLR and neural network techniques. *J. Mar. Syst.* **111–112**: 11–18.
975 doi:10.1016/j.jmarsys.2012.09.002

976 Waugh, D. W., T. M. Hall, B. I. Mcneil, R. Key, and R. J. Matear. 2006. Anthropogenic CO₂ in
977 the oceans estimated using transit time distributions. *Tellus B Chem. Phys. Meteorol.* **58**:
978 376–389. doi:10.1111/j.1600-0889.2006.00222.x

979 Williams, N. L., L. W. Juranek, R. A. Feely, and others. 2017. Calculating surface ocean pCO_2
 980 from biogeochemical Argo floats equipped with pH: An uncertainty analysis. *Global*
 981 *Biogeochem. Cycles* **31**: 591–604. doi:10.1002/2016GB005541

982 Williams, N. L., L. W. Juranek, R. A. Feely, J. L. Russell, K. S. Johnson, and B. Hales. 2018.
 983 Assessment of the Carbonate Chemistry Seasonal Cycles in the Southern Ocean From
 984 Persistent Observational Platforms. *J. Geophys. Res. Ocean.* **123**.
 985 doi:10.1029/2017JC012917

986 Williams, N. L., L. W. Juranek, K. S. Johnson, and others. 2016. Empirical algorithms to
 987 estimate water column pH in the Southern Ocean. *Geophys. Res. Lett.* **43**: 3415–3422.
 988 doi:10.1002/2016GL068539

989 Woosley, R. J., F. J. Millero, and R. Wanninkhof. 2016. Rapid Anthropogenic Changes in CO_2
 990 and pH in the Atlantic Ocean: 2003–2014. *Global Biogeochem. Cycles* **30**: 1–21.
 991 doi:10.1002/2015GB005248

992

993 **12. Figures and Tables**

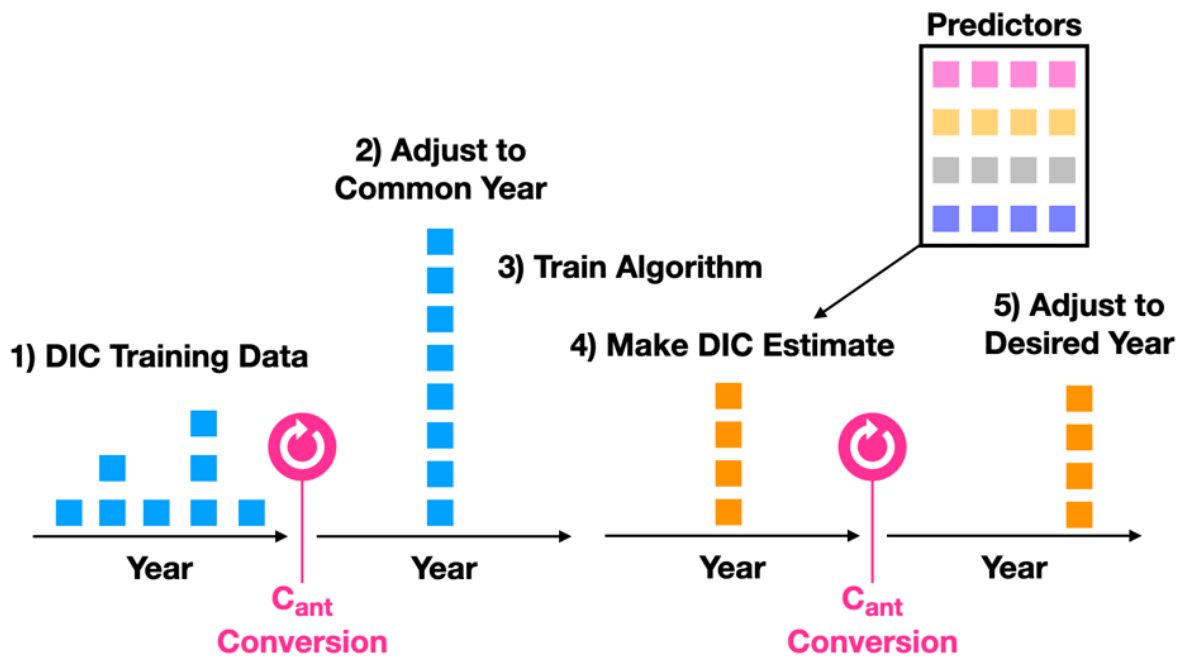


Figure 1. A schematic showing the approach for adjusting training data and estimates for effects of anthropogenic carbon accumulation. The “common year” is 2002.

994

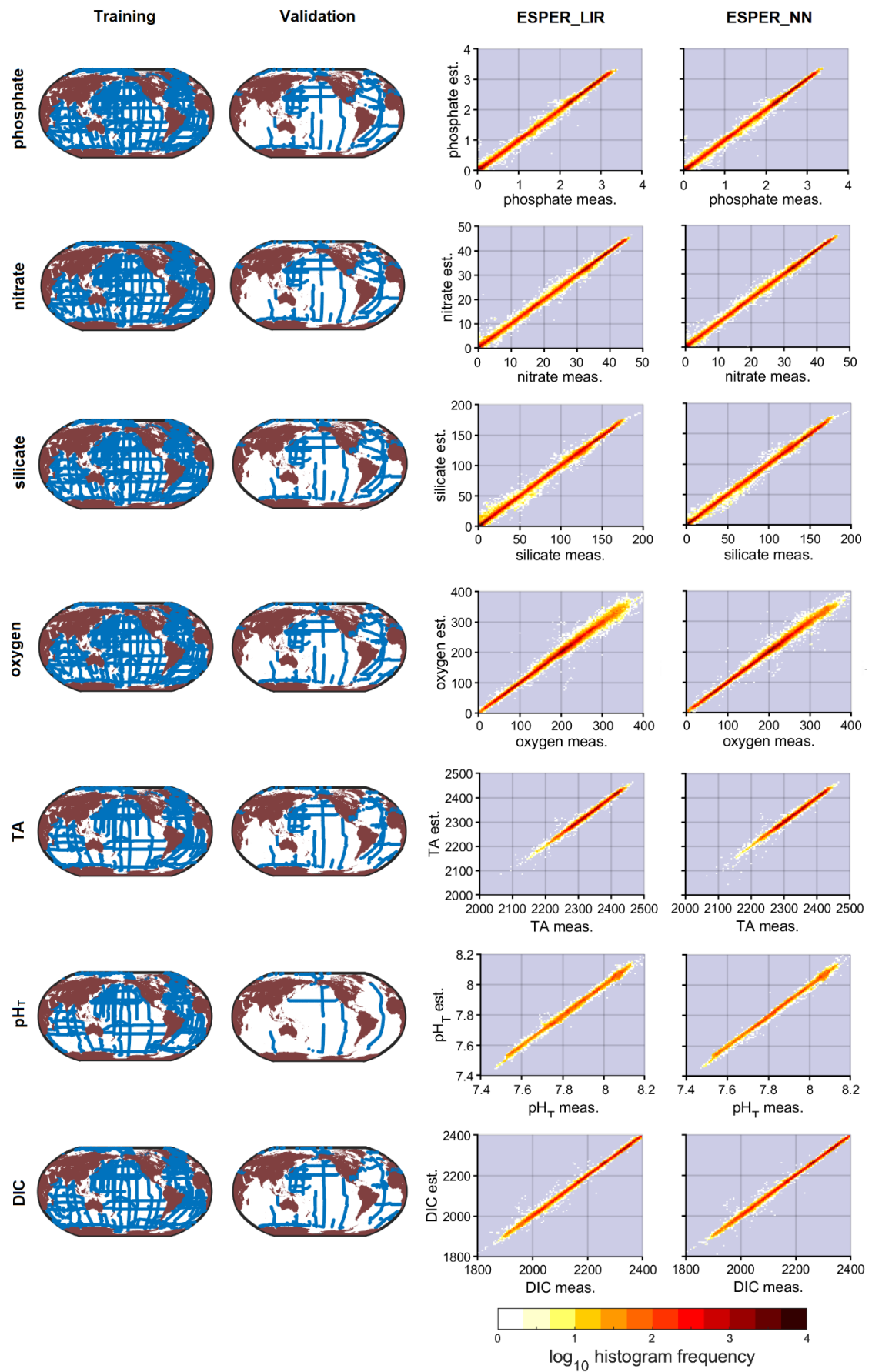


Figure 2. The first column contains maps of the measurement locations used to train the ESPER_LIR_validation and ESPER_NN_validation algorithms. The second column maps the validation data used to assess these versions of the algorithms. The final ESPER_NN and ESPER_LIR algorithms are trained with data shown in both rows of maps. Panels in the right two columns are two-dimensional histograms showing the number of measurements that fall within bins of measured (x-axes) and estimated (with Eqn. 1 from Table 2, y-axes) values of the indicated properties for ESPER_LIR. Color indicates the number of measurements in each bin (bins are small enough as to appear to be pixels), with darker colors indicating more measurements. The rightmost column is the same as the 3rd column from the left, but for ESPER_NN property estimates. An ideal algorithm would have darker colored boxes along the 1:1 lines in the first two rows.

995

- All
- Southern Ocean
- Arctic
- Sea of Japan
- North Atlantic
- Equatorial Pacific
- Mediterranean
- Gulf of Mexico
- California Current

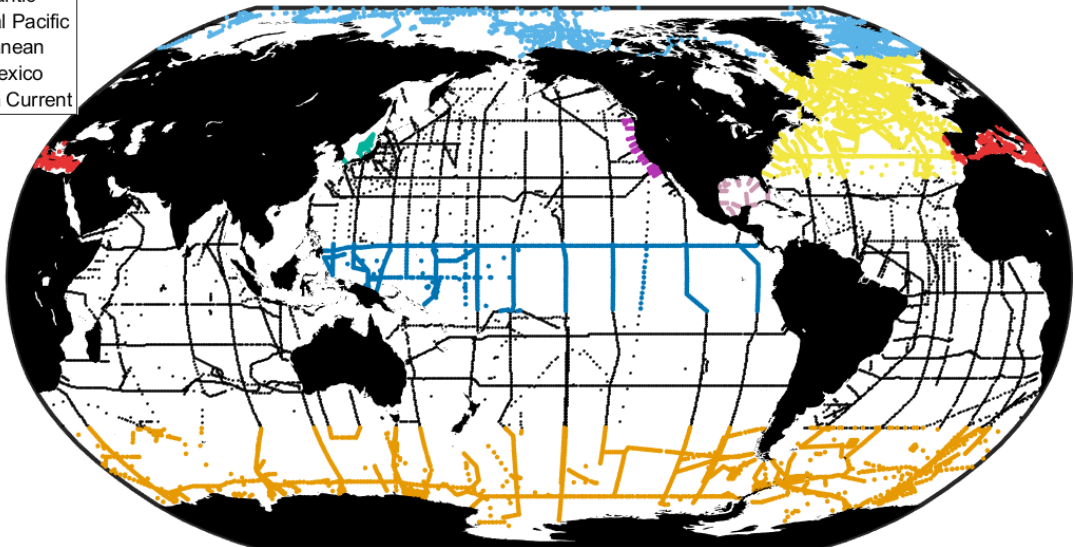


Figure 3. A map showing the regions considered independently in Sect. 3.6.

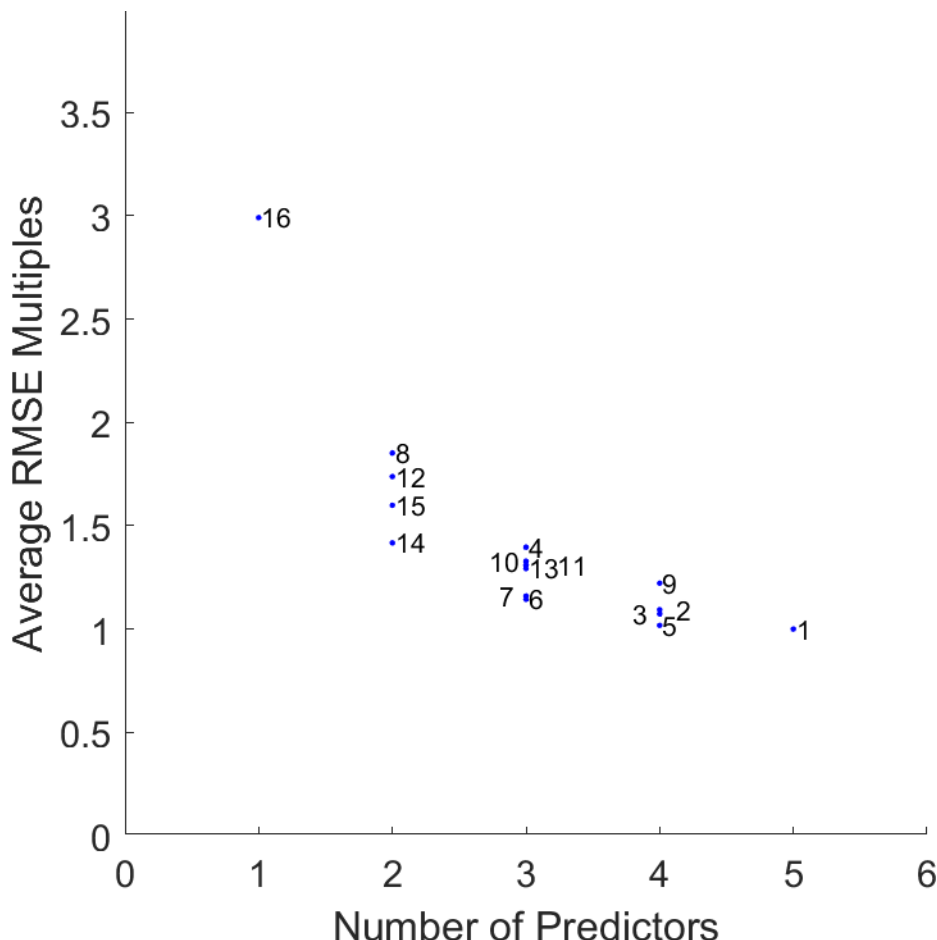


Figure 4. The average global RMSE across all property estimates for both ESPER variants normalized to the RMSE of the equation with the lowest average global RMSE (equation 1) and plotted against the number of predictors required for each estimate (x-axis). The point labels correspond to the equation numbers in Table 2. RMSE generally decreases as the number of predictors increases, but not all predictors have the same predictive power and the incremental increase in predictive power diminishes when more than 3 predictors are used.

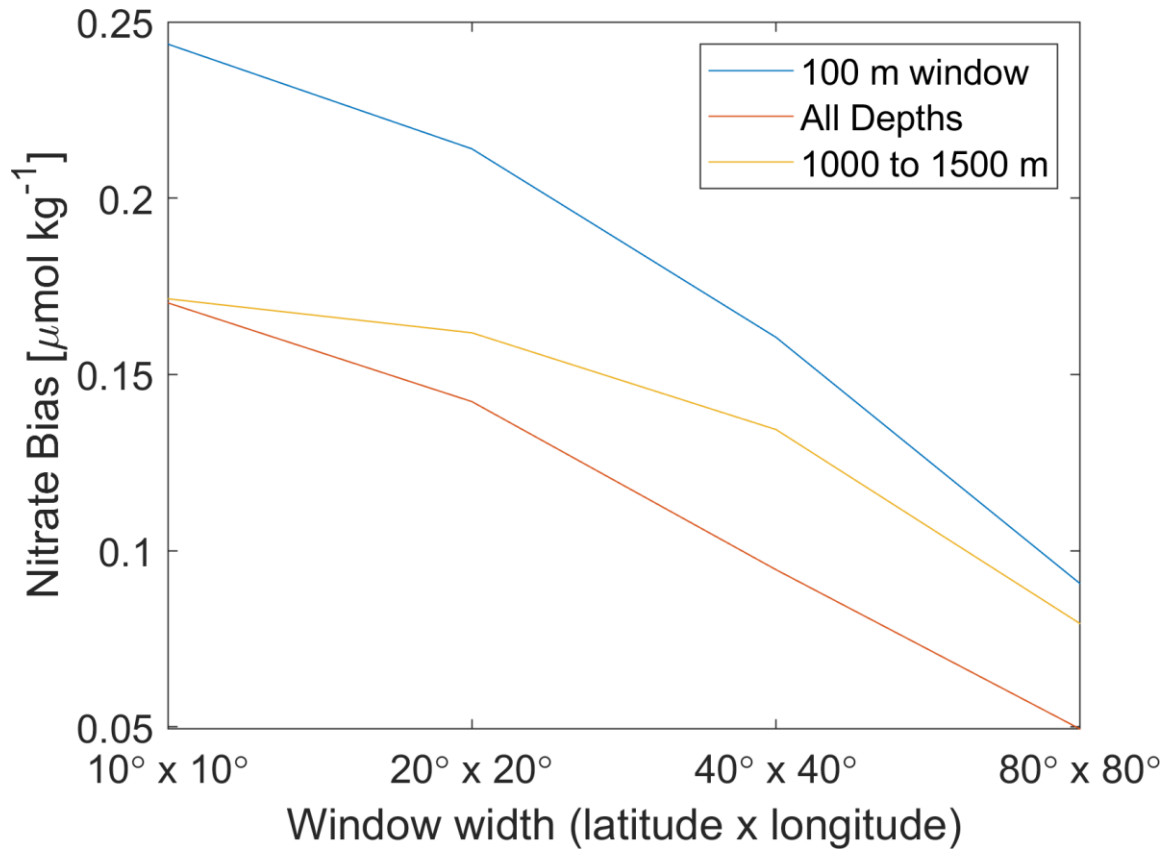


Figure 5. Average absolute bias in ESPER_NN_validation equation-7 nitrate estimates (y-axis) vs. the size of the latitude and longitude windows (x-axis) over which the average of the absolute biases was computed. The three lines correspond to bias estimates that were averaged over a narrow 100 m depth window (blue line), over all depths (orange), and over the 1000 to 1500 m depth range commonly used for float calibration (red). Biases are area-weighted average estimates for each of the grid locations used by the ESPER_NN routine. Nitrate eqn. 7 is chosen as this is one of the equations that is used to calibrate and validate nitrate sensors on biogeochemical Argo floats.

Table 1. Numbers of viable measurement combinations available for each property within the indicated data product subsets. The “total” column reflects the training data for the released routines, whereas the “GLODAPv2” column reflects the training data for the validation routines used to assess the algorithms against New/Assessment data.

Property	GLODAPv2	New/Assessment	Total
Phosphate	540511	146263	711347
Nitrate	540511	146263	711347
Silicate	540511	146263	711347
Oxygen	540511	146263	711347
TA	203502	71832	286080
pH	162783	53615	222822
DIC	244062	71326	323328

Table 2. The combinations of predictors used to estimate each property for each of the 16 equations. Rows with a checkmark indicate the predictors (listed above by property) are included in that equation for that property.

Property	Predictor 1	Predictor 2	Predictor 3	Predictor 4	Predictor 5
Phosphate	S	θ	Nitrate	Oxygen	Silicate
Nitrate	S	θ	Phosphate	Oxygen	Silicate
Silicate	S	θ	Phosphate	Oxygen	Nitrate
Oxygen	S	θ	Phosphate	Nitrate	Silicate
TA	S	θ	Nitrate	Oxygen	Silicate
pH	S	θ	Nitrate	Oxygen	Silicate
DIC	S	θ	Nitrate	Oxygen	Silicate
Equation #					
1	✓	✓	✓	✓	✓
2	✓	✓	✓		✓
3	✓	✓		✓	✓
4	✓	✓			✓
5	✓	✓	✓	✓	
6	✓	✓	✓		
7	✓	✓		✓	
8	✓	✓			
9	✓		✓	✓	✓
10	✓		✓		✓
11	✓			✓	✓
12	✓				✓
13	✓		✓	✓	
14	✓		✓		
15	✓			✓	
16	✓				

Table 3. Assumed default measurement uncertainties, or $E_{Pi_Default}$ or $E_{X_Default}$ as defined in the text.

Property	Uncertainty	Units
S	0.003	
θ	0.003	°C
Phosphate	2%	$\mu\text{mol kg}^{-1}$
Nitrate	2%	$\mu\text{mol kg}^{-1}$
Silicate	2%	$\mu\text{mol kg}^{-1}$
Oxygen	1%	$\mu\text{mol kg}^{-1}$

Table 4. Assessment statistics, reported as bias (\pm RMSE) in $\mu\text{mol kg}^{-1}$, for various phosphate estimation routines presented both globally (top rows) and for intermediate ocean depths (bottom rows, provided for comparison only as there are no float-based phosphate sensors calibrated using algorithms). The equation numbers are specific to the LIR approach, but the equivalent seawater property predictors are used for the other algorithms in the same row.

Global	LIRv2	ESPER_LIR	ESPER_NN	CANYON-B	Mixed
N	146263	146263	146263	146263	146263
Eqn. 1	0.002 (\pm 0.035)	0.001 (\pm 0.036)	0.001 (\pm 0.036)	-	0.003 (\pm 0.039)
Eqn. 2	0.001 (\pm 0.039)	0.000 (\pm 0.038)	0.001 (\pm 0.037)	-	0.002 (\pm 0.039)
Eqn. 3	0.003 (\pm 0.044)	0.001 (\pm 0.044)	0.001 (\pm 0.040)	-	0.003 (\pm 0.042)
Eqn. 4	-0.001 (\pm 0.061)	-0.006 (\pm 0.060)	-0.003 (\pm 0.053)	-	0.000 (\pm 0.045)
Eqn. 5	0.002 (\pm 0.036)	0.001 (\pm 0.037)	0.002 (\pm 0.036)	-	0.003 (\pm 0.039)
Eqn. 6	0.001 (\pm 0.041)	-0.001 (\pm 0.039)	0.001 (\pm 0.038)	-	0.002 (\pm 0.039)
Eqn. 7	0.005 (\pm 0.052)	0.004 (\pm 0.051)	0.003 (\pm 0.043)	0.004 (\pm 0.043)	0.004 (\pm 0.045)
Eqn. 8	-0.003 (\pm 0.089)	-0.003 (\pm 0.086)	-0.002 (\pm 0.075)	-	0.001 (\pm 0.053)
Eqn. 9	0.003 (\pm 0.036)	0.002 (\pm 0.037)	0.002 (\pm 0.036)	-	0.003 (\pm 0.039)
Eqn. 10	0.002 (\pm 0.040)	0.000 (\pm 0.039)	0.001 (\pm 0.039)	-	0.002 (\pm 0.038)
Eqn. 11	0.005 (\pm 0.048)	0.002 (\pm 0.049)	0.002 (\pm 0.044)	-	0.003 (\pm 0.043)
Eqn. 12	-0.003 (\pm 0.079)	-0.006 (\pm 0.065)	-0.003 (\pm 0.057)	-	0.001 (\pm 0.046)
Eqn. 13	0.004 (\pm 0.037)	0.002 (\pm 0.038)	0.003 (\pm 0.037)	-	0.003 (\pm 0.039)
Eqn. 14	0.002 (\pm 0.043)	0.000 (\pm 0.040)	0.002 (\pm 0.040)	-	0.003 (\pm 0.039)
Eqn. 15	0.011 (\pm 0.069)	0.008 (\pm 0.067)	0.007 (\pm 0.059)	-	0.005 (\pm 0.051)
Eqn. 16	0.008 (\pm 0.152)	0.005 (\pm 0.141)	0.004 (\pm 0.129)	-	0.004 (\pm 0.078)
<i>Intermediate depth only (i.e., >1000 m and <1500 m depth)</i>					
N	14397	14397	14397	14397	14397
Eqn. 1	0.009 (\pm 0.030)	0.007 (\pm 0.030)	0.007 (\pm 0.028)	-	0.007 (\pm 0.029)
Eqn. 2	0.009 (\pm 0.031)	0.006 (\pm 0.030)	0.008 (\pm 0.030)	-	0.008 (\pm 0.029)
Eqn. 3	0.011 (\pm 0.032)	0.008 (\pm 0.032)	0.009 (\pm 0.030)	-	0.008 (\pm 0.030)
Eqn. 4	0.012 (\pm 0.040)	0.007 (\pm 0.038)	0.006 (\pm 0.036)	-	0.007 (\pm 0.031)
Eqn. 5	0.010 (\pm 0.029)	0.007 (\pm 0.029)	0.008 (\pm 0.029)	-	0.008 (\pm 0.029)
Eqn. 6	0.009 (\pm 0.030)	0.006 (\pm 0.030)	0.008 (\pm 0.030)	-	0.008 (\pm 0.029)
Eqn. 7	0.011 (\pm 0.031)	0.008 (\pm 0.031)	0.010 (\pm 0.030)	0.011 (\pm 0.031)	0.009 (\pm 0.030)
Eqn. 8	0.012 (\pm 0.044)	0.003 (\pm 0.041)	0.005 (\pm 0.046)	-	0.007 (\pm 0.034)
Eqn. 9	0.009 (\pm 0.030)	0.007 (\pm 0.030)	0.007 (\pm 0.029)	-	0.008 (\pm 0.029)
Eqn. 10	0.009 (\pm 0.031)	0.006 (\pm 0.030)	0.005 (\pm 0.029)	-	0.006 (\pm 0.028)
Eqn. 11	0.011 (\pm 0.032)	0.008 (\pm 0.032)	0.009 (\pm 0.031)	-	0.008 (\pm 0.030)
Eqn. 12	0.012 (\pm 0.046)	0.005 (\pm 0.038)	0.005 (\pm 0.038)	-	0.007 (\pm 0.032)
Eqn. 13	0.010 (\pm 0.030)	0.007 (\pm 0.029)	0.007 (\pm 0.029)	-	0.007 (\pm 0.029)
Eqn. 14	0.009 (\pm 0.031)	0.006 (\pm 0.030)	0.007 (\pm 0.030)	-	0.007 (\pm 0.028)
Eqn. 15	0.012 (\pm 0.033)	0.008 (\pm 0.031)	0.010 (\pm 0.032)	-	0.009 (\pm 0.031)
Eqn. 16	0.013 (\pm 0.056)	0.000 (\pm 0.049)	0.002 (\pm 0.053)	-	0.005 (\pm 0.037)

Table 5. Assessment statistics, reported as bias \pm (RMSE) in $\mu\text{mol kg}^{-1}$, for various nitrate estimation routines presented both globally (top rows) and for the intermediate ocean where float-based sensor measurements are often checked against algorithm-based estimates (bottom rows).

Global	LIRv2	ESPER_LIR	ESPER_NN	CANYON-B	Mixed
N	146263	146263	146263	146263	146263
Eqn. 1	0.03 (± 0.52)	0.02 (± 0.48)	0.00 (± 0.42)	-	0.03 (± 0.49)
Eqn. 2	0.01 (± 0.56)	0.00 (± 0.52)	-0.01 (± 0.47)	-	0.03 (± 0.49)
Eqn. 3	0.04 (± 0.61)	0.01 (± 0.59)	0.00 (± 0.50)	-	0.03 (± 0.55)
Eqn. 4	-0.02 (± 0.86)	-0.09 (± 0.82)	-0.07 (± 0.72)	-	0.00 (± 0.59)
Eqn. 5	0.03 (± 0.54)	0.03 (± 0.49)	0.02 (± 0.43)	-	0.04 (± 0.50)
Eqn. 6	0.00 (± 0.58)	-0.01 (± 0.55)	-0.01 (± 0.50)	-	0.03 (± 0.50)
Eqn. 7	0.06 (± 0.72)	0.06 (± 0.70)	0.03 (± 0.56)	0.03 (± 0.56)	0.04 (± 0.59)
Eqn. 8	-0.06 (± 1.26)	-0.04 (± 1.21)	-0.05 (± 1.04)	-	0.01 (± 0.73)
Eqn. 9	0.03 (± 0.54)	0.02 (± 0.50)	0.01 (± 0.44)	-	0.04 (± 0.50)
Eqn. 10	0.00 (± 0.58)	-0.01 (± 0.54)	-0.01 (± 0.49)	-	0.03 (± 0.50)
Eqn. 11	0.05 (± 0.67)	0.02 (± 0.65)	0.00 (± 0.57)	-	0.03 (± 0.56)
Eqn. 12	-0.08 (± 1.21)	-0.10 (± 0.89)	-0.06 (± 0.77)	-	0.00 (± 0.60)
Eqn. 13	0.05 (± 0.57)	0.04 (± 0.52)	0.03 (± 0.48)	-	0.05 (± 0.52)
Eqn. 14	0.00 (± 0.62)	0.00 (± 0.57)	-0.01 (± 0.53)	-	0.03 (± 0.51)
Eqn. 15	0.12 (± 0.96)	0.11 (± 0.91)	0.08 (± 0.81)	-	0.07 (± 0.69)
Eqn. 16	0.06 (± 2.22)	0.06 (± 2.00)	0.02 (± 1.83)	-	0.04 (± 1.08)
<i>Intermediate depth only (i.e., >1000 m and <1500 m depth)</i>					
N	14397	14397	14397	14397	14397
Eqn. 1	-0.01 (± 0.32)	-0.01 (± 0.31)	-0.01 (± 0.29)	-	0.01 (± 0.30)
Eqn. 2	-0.04 (± 0.36)	-0.05 (± 0.34)	-0.04 (± 0.34)	-	-0.01 (± 0.30)
Eqn. 3	0.03 (± 0.33)	0.02 (± 0.32)	0.02 (± 0.31)	-	0.02 (± 0.31)
Eqn. 4	0.05 (± 0.45)	0.01 (± 0.40)	-0.01 (± 0.44)	-	0.00 (± 0.34)
Eqn. 5	-0.01 (± 0.33)	-0.02 (± 0.32)	0.00 (± 0.30)	-	0.01 (± 0.30)
Eqn. 6	-0.05 (± 0.38)	-0.08 (± 0.38)	-0.07 (± 0.38)	-	-0.02 (± 0.31)
Eqn. 7	0.04 (± 0.34)	0.02 (± 0.33)	0.04 (± 0.33)	0.04 (± 0.33)	0.03 (± 0.32)
Eqn. 8	0.05 (± 0.54)	-0.05 (± 0.53)	-0.01 (± 0.58)	-	0.01 (± 0.40)
Eqn. 9	-0.01 (± 0.32)	-0.02 (± 0.32)	0.00 (± 0.30)	-	0.01 (± 0.30)
Eqn. 10	-0.05 (± 0.37)	-0.07 (± 0.37)	-0.07 (± 0.34)	-	-0.02 (± 0.30)
Eqn. 11	0.03 (± 0.34)	0.02 (± 0.32)	0.03 (± 0.32)	-	0.02 (± 0.31)
Eqn. 12	0.04 (± 0.55)	-0.03 (± 0.45)	-0.02 (± 0.46)	-	0.00 (± 0.35)
Eqn. 13	-0.01 (± 0.34)	-0.02 (± 0.33)	-0.01 (± 0.32)	-	0.01 (± 0.31)
Eqn. 14	-0.06 (± 0.40)	-0.10 (± 0.39)	-0.07 (± 0.40)	-	-0.03 (± 0.32)
Eqn. 15	0.05 (± 0.37)	0.02 (± 0.34)	0.03 (± 0.36)	-	0.03 (± 0.33)
Eqn. 16	0.06 (± 0.73)	-0.09 (± 0.65)	-0.06 (± 0.71)	-	-0.02 (± 0.45)

Table 6. Assessment statistics, reported as bias \pm (RMSE) in $\mu\text{mol kg}^{-1}$, for various silicate estimation routines presented both globally (top rows) and for the intermediate ocean (bottom rows, provided for comparison only as there are no float-based sensors for phosphate that are calibrated using algorithms).

Global	LIRv2	ESPER_LIR	ESPER_NN	CANYON-B	Mixed
N	146263	146263	146263	146263	146263
Eqn. 1	-0.3 (± 2.4)	0.0 (± 2.2)	0.0 (± 1.8)	-	0.1 (± 1.9)
Eqn. 2	-0.3 (± 2.5)	-0.1 (± 2.5)	-0.1 (± 2.1)	-	0.0 (± 2.0)
Eqn. 3	-0.2 (± 2.4)	0.0 (± 2.2)	0.1 (± 2.0)	-	0.1 (± 2.0)
Eqn. 4	-0.3 (± 2.6)	-0.1 (± 2.5)	0.0 (± 2.0)	-	0.1 (± 2.0)
Eqn. 5	-0.2 (± 2.4)	0.0 (± 2.3)	0.1 (± 1.8)	-	0.1 (± 1.9)
Eqn. 6	-0.3 (± 2.7)	-0.2 (± 2.6)	-0.1 (± 2.1)	-	0.0 (± 2.0)
Eqn. 7	-0.2 (± 2.7)	0.1 (± 2.3)	0.1 (± 2.0)	0.1 (± 1.9)	0.1 (± 2.0)
Eqn. 8	-0.3 (± 3.6)	-0.1 (± 3.3)	-0.1 (± 2.7)	-	0.0 (± 2.2)
Eqn. 9	0.0 (± 4.1)	0.1 (± 3.0)	0.1 (± 2.6)	-	0.1 (± 2.2)
Eqn. 10	-0.1 (± 5.0)	0.1 (± 3.1)	0.0 (± 2.6)	-	0.0 (± 2.2)
Eqn. 11	0.0 (± 4.3)	0.1 (± 3.0)	0.1 (± 2.6)	-	0.1 (± 2.1)
Eqn. 12	0.0 (± 4.9)	0.1 (± 3.1)	0.0 (± 2.7)	-	0.1 (± 2.2)
Eqn. 13	0.1 (± 4.6)	0.1 (± 3.2)	0.1 (± 2.7)	-	0.1 (± 2.2)
Eqn. 14	-0.1 (± 5.2)	0.0 (± 3.3)	-0.1 (± 2.8)	-	0.0 (± 2.2)
Eqn. 15	0.3 (± 5.5)	0.3 (± 3.4)	0.2 (± 3.2)	-	0.2 (± 2.4)
Eqn. 16	0.4 (± 6.9)	0.1 (± 5.4)	-0.1 (± 5.3)	-	0.0 (± 3.2)
<i>Intermediate depth only (i.e., >1000 m and <1500 m depth)</i>					
N	14397	14397	14397	14397	14397
Eqn. 1	-0.3 (± 2.0)	-0.2 (± 1.7)	-0.1 (± 1.6)	-	-0.1 (± 1.5)
Eqn. 2	-0.3 (± 2.1)	-0.3 (± 2.1)	-0.2 (± 2.0)	-	-0.2 (± 1.6)
Eqn. 3	-0.3 (± 2.0)	-0.1 (± 1.6)	-0.1 (± 1.7)	-	-0.1 (± 1.5)
Eqn. 4	-0.3 (± 2.1)	-0.2 (± 1.9)	-0.1 (± 1.9)	-	-0.1 (± 1.6)
Eqn. 5	-0.3 (± 2.1)	-0.2 (± 1.8)	-0.1 (± 1.6)	-	-0.1 (± 1.5)
Eqn. 6	-0.3 (± 2.3)	-0.5 (± 2.4)	-0.3 (± 2.0)	-	-0.2 (± 1.6)
Eqn. 7	-0.3 (± 2.1)	-0.1 (± 1.6)	-0.2 (± 1.7)	0.0 (± 1.5)	-0.2 (± 1.5)
Eqn. 8	-0.1 (± 2.7)	-0.3 (± 2.6)	-0.1 (± 2.4)	-	-0.1 (± 1.7)
Eqn. 9	0.0 (± 3.4)	-0.1 (± 3.3)	-0.2 (± 3.3)	-	-0.2 (± 2.2)
Eqn. 10	0.0 (± 5.7)	-0.1 (± 3.2)	-0.2 (± 3.3)	-	-0.2 (± 2.1)
Eqn. 11	0.0 (± 3.7)	-0.1 (± 2.9)	-0.1 (± 3.4)	-	-0.1 (± 2.2)
Eqn. 12	0.1 (± 5.5)	0.0 (± 3.0)	0.0 (± 3.3)	-	-0.1 (± 2.1)
Eqn. 13	0.0 (± 4.1)	-0.1 (± 3.7)	-0.3 (± 3.4)	-	-0.2 (± 2.2)
Eqn. 14	-0.1 (± 6.4)	-0.4 (± 3.4)	-0.4 (± 3.6)	-	-0.3 (± 2.3)
Eqn. 15	0.1 (± 5.3)	0.0 (± 3.2)	-0.1 (± 3.8)	-	-0.1 (± 2.3)
Eqn. 16	0.2 (± 6.1)	-0.4 (± 4.0)	-0.1 (± 4.7)	-	-0.1 (± 2.7)

Table 7. Assessment statistics, reported as bias \pm (RMSE) in $\mu\text{mol kg}^{-1}$, for various oxygen estimation routines presented both globally (top rows) and for the intermediate ocean (bottom rows, provided for comparison only as float-based oxygen sensors are not commonly quality controlled against algorithms).

Global	LIRv2	ESPER_LIR	ESPER_NN	CANYON-B [†]	Mixed
N	146263	146263	146263	†	146263
Eqn. 1	0.5 (± 5.3)	0.6 (± 5.2)	0.5 (± 4.5)	-	0.6 (± 4.7)
Eqn. 2	0.4 (± 5.7)	0.5 (± 5.6)	0.5 (± 5.0)	-	0.6 (± 4.8)
Eqn. 3	0.5 (± 5.8)	0.6 (± 5.5)	0.6 (± 4.8)	-	0.6 (± 4.9)
Eqn. 4	0.7 (± 8.0)	1.3 (± 7.6)	1.0 (± 7.1)	-	0.8 (± 5.6)
Eqn. 5	0.6 (± 5.5)	0.8 (± 5.4)	0.7 (± 4.7)	-	0.7 (± 4.8)
Eqn. 6	0.7 (± 5.9)	0.8 (± 5.8)	0.6 (± 5.3)	-	0.7 (± 4.8)
Eqn. 7	0.6 (± 6.2)	0.7 (± 5.6)	0.5 (± 5.0)	-	0.6 (± 5.0)
Eqn. 8	1.1 (± 10.8)	1.2 (± 10.0)	1.1 (± 9.7)	-	0.9 (± 6.6)
Eqn. 9	1.1 (± 8.1)	1.0 (± 7.9)	1.1 (± 7.0)	-	0.9 (± 5.6)
Eqn. 10	1.1 (± 8.8)	1.0 (± 8.3)	1.1 (± 7.6)	-	0.9 (± 5.7)
Eqn. 11	1.1 (± 8.4)	1.0 (± 8.0)	1.0 (± 7.4)	-	0.9 (± 5.8)
Eqn. 12	2.0 (± 14.2)	1.7 (± 9.9)	1.4 (± 9.5)	-	1.1 (± 6.5)
Eqn. 13	1.4 (± 9.8)	1.3 (± 8.2)	1.1 (± 7.3)	-	0.9 (± 5.7)
Eqn. 14	1.5 (± 10.4)	1.3 (± 8.4)	1.2 (± 7.7)	-	1.0 (± 5.8)
Eqn. 15	1.4 (± 9.8)	1.2 (± 8.2)	1.0 (± 7.6)	-	0.9 (± 5.9)
Eqn. 16	1.6 (± 18.6)	1.2 (± 13.7)	0.8 (± 13.1)	-	0.8 (± 7.9)
<i>Intermediate depth only (i.e., >1000 m and <1500 m depth)</i>					
N	14397	14397	14397	†	14397
Eqn. 1	0.2 (± 2.8)	0.4 (± 2.6)	0.6 (± 2.7)	-	0.5 (± 2.6)
Eqn. 2	0.4 (± 3.4)	0.7 (± 2.9)	0.8 (± 3.1)	-	0.6 (± 2.6)
Eqn. 3	0.0 (± 3.0)	0.2 (± 2.6)	0.1 (± 2.8)	-	0.3 (± 2.6)
Eqn. 4	-0.4 (± 4.3)	0.2 (± 3.3)	0.1 (± 4.2)	-	0.3 (± 2.9)
Eqn. 5	0.4 (± 3.0)	0.6 (± 2.9)	0.8 (± 3.1)	-	0.6 (± 2.8)
Eqn. 6	0.6 (± 3.8)	1.1 (± 3.5)	1.1 (± 3.9)	-	0.8 (± 3.0)
Eqn. 7	0.0 (± 3.2)	0.4 (± 2.9)	0.4 (± 3.1)	-	0.4 (± 2.8)
Eqn. 8	-0.3 (± 5.1)	0.8 (± 4.8)	0.2 (± 5.9)	-	0.3 (± 3.7)
Eqn. 9	0.4 (± 3.8)	0.8 (± 3.9)	1.0 (± 3.6)	-	0.7 (± 3.0)
Eqn. 10	0.7 (± 4.2)	1.2 (± 4.7)	1.2 (± 4.1)	-	0.8 (± 3.0)
Eqn. 11	0.2 (± 3.9)	0.6 (± 3.8)	0.7 (± 4.0)	-	0.6 (± 3.1)
Eqn. 12	-0.2 (± 6.1)	0.7 (± 4.8)	0.4 (± 5.4)	-	0.4 (± 3.4)
Eqn. 13	0.7 (± 5.4)	1.0 (± 4.0)	0.8 (± 4.0)	-	0.6 (± 3.1)
Eqn. 14	1.1 (± 5.7)	1.5 (± 4.5)	1.2 (± 4.4)	-	0.8 (± 3.1)
Eqn. 15	0.4 (± 5.5)	0.8 (± 4.0)	0.6 (± 4.3)	-	0.5 (± 3.2)
Eqn. 16	0.0 (± 7.6)	1.4 (± 6.2)	0.2 (± 6.0)	-	0.3 (± 3.7)

[†]This routine does not estimate this quantity

Table 8. Assessment statistics, reported as bias \pm (RMSE) in $\mu\text{mol kg}^{-1}$, for various TA estimation routines presented both globally (top rows) and for the intermediate ocean (bottom rows, provided for comparison only as TA sensors have yet to be widely deployed on floats).

Global	LIRv2	ESPER_LIR	ESPER_NN	CANYON-B	Mixed
N	71832	71832	71832	71832	71832
Eqn. 1	0.8 (± 3.6)	0.8 (± 3.6)	0.8 (± 3.7)	-	0.8 (± 3.5)
Eqn. 2	0.7 (± 3.6)	0.8 (± 3.6)	0.8 (± 3.7)	-	0.8 (± 3.5)
Eqn. 3	0.7 (± 3.7)	0.8 (± 3.6)	0.8 (± 3.7)	-	0.7 (± 3.5)
Eqn. 4	0.7 (± 3.7)	0.9 (± 3.6)	0.9 (± 3.8)	-	0.8 (± 3.6)
Eqn. 5	0.5 (± 3.9)	0.6 (± 3.7)	0.7 (± 3.7)	-	0.7 (± 3.6)
Eqn. 6	0.4 (± 4.0)	0.5 (± 3.8)	0.7 (± 3.9)	-	0.7 (± 3.6)
Eqn. 7	0.5 (± 4.0)	0.7 (± 3.7)	0.8 (± 3.8)	0.4 (± 4.2)	0.7 (± 3.6)
Eqn. 8	0.5 (± 4.3)	0.6 (± 4.0)	0.8 (± 4.1)	-	0.7 (± 3.7)
Eqn. 9	0.7 (± 3.7)	0.8 (± 3.7)	0.9 (± 3.7)	-	0.8 (± 3.5)
Eqn. 10	0.7 (± 3.7)	0.9 (± 3.7)	0.9 (± 3.7)	-	0.8 (± 3.5)
Eqn. 11	0.7 (± 3.7)	0.9 (± 3.7)	0.9 (± 3.6)	-	0.8 (± 3.5)
Eqn. 12	0.8 (± 3.9)	1.0 (± 3.7)	0.9 (± 3.7)	-	0.8 (± 3.5)
Eqn. 13	0.7 (± 4.4)	0.8 (± 3.9)	0.8 (± 4.0)	-	0.7 (± 3.6)
Eqn. 14	0.7 (± 4.9)	0.7 (± 4.1)	0.8 (± 4.0)	-	0.7 (± 3.6)
Eqn. 15	1.0 (± 4.8)	0.9 (± 4.0)	0.9 (± 4.0)	-	0.8 (± 3.6)
Eqn. 16	1.2 (± 6.5)	0.9 (± 5.0)	0.7 (± 5.2)	-	0.7 (± 4.0)
<i>Intermediate depth only</i> (i.e., >1000 m and <1500 m depth)					
N	6797	6797	6797	6797	6797
Eqn. 1	0.9 (± 3.0)	0.8 (± 2.9)	1.0 (± 3.0)	-	0.8 (± 2.8)
Eqn. 2	0.9 (± 2.9)	0.8 (± 2.9)	0.9 (± 2.9)	-	0.8 (± 2.8)
Eqn. 3	0.9 (± 2.9)	0.8 (± 2.9)	0.9 (± 3.0)	-	0.8 (± 2.8)
Eqn. 4	0.8 (± 3.0)	0.8 (± 2.9)	0.9 (± 3.0)	-	0.8 (± 2.9)
Eqn. 5	0.6 (± 3.2)	0.6 (± 2.9)	0.7 (± 3.1)	-	0.7 (± 2.9)
Eqn. 6	0.6 (± 3.2)	0.5 (± 2.9)	0.8 (± 3.2)	-	0.7 (± 2.9)
Eqn. 7	0.6 (± 3.2)	0.6 (± 2.9)	0.7 (± 3.1)	0.5 (± 3.2)	0.7 (± 2.9)
Eqn. 8	0.7 (± 3.2)	0.6 (± 2.9)	0.8 (± 3.3)	-	0.7 (± 3.0)
Eqn. 9	0.9 (± 3.0)	0.9 (± 2.9)	0.9 (± 3.0)	-	0.8 (± 2.9)
Eqn. 10	0.8 (± 3.0)	0.8 (± 2.9)	1.0 (± 3.1)	-	0.8 (± 2.9)
Eqn. 11	0.9 (± 3.0)	0.9 (± 2.9)	1.0 (± 3.0)	-	0.8 (± 2.9)
Eqn. 12	0.8 (± 3.0)	0.9 (± 2.9)	1.0 (± 3.1)	-	0.8 (± 2.9)
Eqn. 13	0.7 (± 3.8)	0.6 (± 3.2)	0.6 (± 3.6)	-	0.6 (± 3.1)
Eqn. 14	0.7 (± 4.1)	0.5 (± 3.2)	0.6 (± 3.6)	-	0.6 (± 3.1)
Eqn. 15	0.8 (± 3.8)	0.6 (± 3.2)	0.8 (± 3.7)	-	0.7 (± 3.1)
Eqn. 16	0.9 (± 4.4)	0.6 (± 3.4)	0.7 (± 4.5)	-	0.6 (± 3.3)

Table 9. Assessment statistics, reported as bias \pm (RMSE), for various pH estimation routines presented both globally (top rows) and for the intermediate ocean where float-based sensor measurements are often checked against algorithm-based estimates (bottom rows). Only measurements made with purified dyes were used in these assessments to ensure the validation data had no adjustments beyond those applied in the GLODAPv2.2020 secondary quality control process.

Global	LIRv2	ESPER_LIR	ESPER_NN	CANYON-B	Mixed
N	20181	20181	20181	20181	20181
Eqn. 1	-0.007 (\pm 0.012)	-0.004 (\pm 0.013)	-0.004 (\pm 0.011)	-	-0.004 (\pm 0.011)
Eqn. 2	-0.006 (\pm 0.015)	-0.002 (\pm 0.014)	-0.002 (\pm 0.013)	-	-0.003 (\pm 0.011)
Eqn. 3	-0.007 (\pm 0.013)	-0.004 (\pm 0.013)	-0.004 (\pm 0.011)	-	-0.004 (\pm 0.011)
Eqn. 4	-0.005 (\pm 0.022)	-0.001 (\pm 0.017)	-0.002 (\pm 0.016)	-	-0.003 (\pm 0.012)
Eqn. 5	-0.007 (\pm 0.012)	-0.004 (\pm 0.012)	-0.004 (\pm 0.011)	-	-0.004 (\pm 0.011)
Eqn. 6	-0.005 (\pm 0.015)	-0.001 (\pm 0.014)	-0.002 (\pm 0.014)	-	-0.003 (\pm 0.011)
Eqn. 7	-0.007 (\pm 0.013)	-0.004 (\pm 0.013)	-0.004 (\pm 0.011)	*	-0.004 (\pm 0.011)
Eqn. 8	-0.005 (\pm 0.026)	0.000 (\pm 0.020)	0.000 (\pm 0.021)	-	-0.002 (\pm 0.014)
Eqn. 9	-0.007 (\pm 0.013)	-0.004 (\pm 0.014)	-0.003 (\pm 0.012)	-	-0.004 (\pm 0.011)
Eqn. 10	-0.005 (\pm 0.016)	-0.002 (\pm 0.015)	-0.001 (\pm 0.014)	-	-0.003 (\pm 0.012)
Eqn. 11	-0.007 (\pm 0.013)	-0.004 (\pm 0.014)	-0.003 (\pm 0.012)	-	-0.004 (\pm 0.011)
Eqn. 12	-0.004 (\pm 0.023)	-0.001 (\pm 0.018)	-0.001 (\pm 0.018)	-	-0.003 (\pm 0.013)
Eqn. 13	-0.006 (\pm 0.013)	-0.004 (\pm 0.013)	-0.003 (\pm 0.012)	-	-0.004 (\pm 0.011)
Eqn. 14	-0.004 (\pm 0.017)	-0.001 (\pm 0.015)	-0.001 (\pm 0.014)	-	-0.003 (\pm 0.012)
Eqn. 15	-0.006 (\pm 0.013)	-0.004 (\pm 0.014)	-0.004 (\pm 0.012)	-	-0.004 (\pm 0.012)
Eqn. 16	-0.005 (\pm 0.033)	-0.001 (\pm 0.026)	-0.002 (\pm 0.027)	-	-0.003 (\pm 0.017)
<i>Intermediate depth only (i.e., >1000 m and <1500 m depth)</i>					
N	2352	2352	2352	2352	2352
Eqn. 1	-0.008 (\pm 0.011)	-0.002 (\pm 0.008)	-0.002 (\pm 0.007)	-	-0.002 (\pm 0.006)
Eqn. 2	-0.007 (\pm 0.013)	-0.001 (\pm 0.008)	-0.001 (\pm 0.008)	-	-0.001 (\pm 0.006)
Eqn. 3	-0.008 (\pm 0.011)	-0.002 (\pm 0.007)	-0.001 (\pm 0.006)	-	-0.001 (\pm 0.006)
Eqn. 4	-0.008 (\pm 0.024)	-0.001 (\pm 0.009)	-0.002 (\pm 0.011)	-	-0.002 (\pm 0.008)
Eqn. 5	-0.008 (\pm 0.011)	-0.002 (\pm 0.007)	-0.002 (\pm 0.007)	-	-0.002 (\pm 0.006)
Eqn. 6	-0.007 (\pm 0.013)	0.001 (\pm 0.008)	0.000 (\pm 0.007)	-	-0.001 (\pm 0.006)
Eqn. 7	-0.008 (\pm 0.011)	-0.002 (\pm 0.007)	-0.002 (\pm 0.007)	*	-0.002 (\pm 0.006)
Eqn. 8	-0.008 (\pm 0.024)	0.001 (\pm 0.009)	0.000 (\pm 0.014)	-	-0.001 (\pm 0.008)
Eqn. 9	-0.007 (\pm 0.011)	-0.002 (\pm 0.008)	-0.001 (\pm 0.006)	-	-0.002 (\pm 0.006)
Eqn. 10	-0.007 (\pm 0.013)	0.001 (\pm 0.008)	0.000 (\pm 0.008)	-	-0.001 (\pm 0.006)
Eqn. 11	-0.007 (\pm 0.011)	-0.002 (\pm 0.007)	-0.001 (\pm 0.007)	-	-0.002 (\pm 0.006)
Eqn. 12	-0.008 (\pm 0.024)	0.000 (\pm 0.010)	0.000 (\pm 0.013)	-	-0.001 (\pm 0.008)
Eqn. 13	-0.007 (\pm 0.011)	-0.002 (\pm 0.007)	-0.002 (\pm 0.007)	-	-0.002 (\pm 0.007)
Eqn. 14	-0.007 (\pm 0.014)	0.001 (\pm 0.007)	0.000 (\pm 0.008)	-	-0.001 (\pm 0.006)
Eqn. 15	-0.007 (\pm 0.011)	-0.001 (\pm 0.007)	-0.001 (\pm 0.007)	-	-0.001 (\pm 0.006)
Eqn. 16	-0.008 (\pm 0.028)	0.002 (\pm 0.010)	0.001 (\pm 0.015)	-	-0.001 (\pm 0.009)

*No viable comparison in this effort due to overlap between training and validation data subsets

Table 10. Assessment statistics, reported as bias (\pm RMSE) in $\mu\text{mol kg}^{-1}$, for various DIC estimation routines presented both globally (top rows) and for the intermediate ocean (bottom rows, provided for comparison only as DIC sensors have yet to be widely deployed on floats).

Global	LIRv2 [†]	ESPER_LIR	ESPER_NN	CANYON-B	Mixed
N	[†]	71326	71326	71326	71326
Eqn. 1	-	0.4 (\pm 5.1)	0.4 (\pm 4.9)	-	0.4 (\pm 4.8)
Eqn. 2	-	0.2 (\pm 5.8)	0.4 (\pm 5.7)	-	0.4 (\pm 4.9)
Eqn. 3	-	0.3 (\pm 4.9)	0.4 (\pm 4.8)	-	0.4 (\pm 4.8)
Eqn. 4	-	-0.2 (\pm 6.6)	0.0 (\pm 6.6)	-	0.2 (\pm 5.2)
Eqn. 5	-	0.3 (\pm 5.1)	0.4 (\pm 5.1)	-	0.4 (\pm 4.9)
Eqn. 6	-	0.0 (\pm 6.1)	0.3 (\pm 6.4)	-	0.3 (\pm 5.2)
Eqn. 7	-	0.4 (\pm 5.3)	0.4 (\pm 5.1)	-1.3 (\pm 5.8)	0.4 (\pm 5.0)
Eqn. 8	-	-0.4 (\pm 8.7)	-0.1 (\pm 8.6)	-	0.1 (\pm 6.0)
Eqn. 9	-	0.6 (\pm 8.2)	0.6 (\pm 6.9)	-	0.5 (\pm 5.3)
Eqn. 10	-	0.3 (\pm 9.0)	0.4 (\pm 7.3)	-	0.4 (\pm 5.3)
Eqn. 11	-	0.5 (\pm 7.4)	0.6 (\pm 6.7)	-	0.5 (\pm 5.3)
Eqn. 12	-	-0.2 (\pm 9.3)	0.1 (\pm 8.5)	-	0.3 (\pm 5.7)
Eqn. 13	-	0.6 (\pm 7.9)	0.7 (\pm 7.3)	-	0.5 (\pm 5.5)
Eqn. 14	-	0.1 (\pm 8.7)	0.3 (\pm 8.0)	-	0.3 (\pm 5.6)
Eqn. 15	-	0.8 (\pm 8.9)	0.8 (\pm 8.4)	-	0.6 (\pm 6.1)
Eqn. 16	-	0.6 (\pm 16.7)	0.3 (\pm 15.7)	-	0.4 (\pm 8.9)
<i>Intermediate depth only (i.e., >1000 m and <1500 m depth)</i>					
N	[†]	6740	6740	6740	ESPER & LIR
Eqn. 1	-	-0.2 (\pm 3.3)	-0.1 (\pm 3.3)	-	-0.2 (\pm 3.3)
Eqn. 2	-	-0.3 (\pm 3.5)	0.0 (\pm 3.7)	-	-0.1 (\pm 3.3)
Eqn. 3	-	-0.2 (\pm 3.3)	0.1 (\pm 3.2)	-	-0.1 (\pm 3.2)
Eqn. 4	-	-0.1 (\pm 3.8)	0.0 (\pm 4.3)	-	-0.1 (\pm 3.5)
Eqn. 5	-	-0.2 (\pm 3.3)	-0.1 (\pm 3.4)	-	-0.2 (\pm 3.3)
Eqn. 6	-	-0.5 (\pm 3.7)	-0.2 (\pm 4.1)	-	-0.2 (\pm 3.5)
Eqn. 7	-	-0.2 (\pm 3.3)	-0.2 (\pm 3.5)	-0.8 (\pm 3.4)	-0.2 (\pm 3.3)
Eqn. 8	-	-0.5 (\pm 4.5)	-0.4 (\pm 5.4)	-	-0.3 (\pm 3.9)
Eqn. 9	-	0.0 (\pm 3.4)	0.1 (\pm 3.3)	-	-0.1 (\pm 3.2)
Eqn. 10	-	-0.2 (\pm 3.5)	-0.1 (\pm 3.7)	-	-0.2 (\pm 3.3)
Eqn. 11	-	-0.1 (\pm 3.4)	0.1 (\pm 3.3)	-	-0.1 (\pm 3.2)
Eqn. 12	-	-0.2 (\pm 3.8)	0.0 (\pm 4.4)	-	-0.1 (\pm 3.5)
Eqn. 13	-	-0.2 (\pm 3.7)	-0.1 (\pm 4.0)	-	-0.2 (\pm 3.5)
Eqn. 14	-	-0.4 (\pm 4.0)	-0.5 (\pm 4.5)	-	-0.4 (\pm 3.6)
Eqn. 15	-	-0.1 (\pm 3.8)	0.0 (\pm 4.2)	-	-0.1 (\pm 3.5)
Eqn. 16	-	-0.7 (\pm 5.7)	-0.3 (\pm 6.8)	-	-0.3 (\pm 4.4)

[†]This routine does not estimate this quantity.

Table 11. Regional assessment statistics for equation 7 of the validation versions of the algorithms and for CANYON-B. These statistics are obtained without including any training data from the new data added in the 2019 and 2020 GLODAPv2 data product updates; without the supplemental data in the Gulf of Mexico; and, in the case of LIRv2, ESPER_LIR, and ESPER_NN, without any measurements in the Mediterranean. The released ESPER_LIR and ESPER_NN routines should perform significantly better in the Sea of Japan/East Sea, the Gulf of Mexico, and the Mediterranean. Statistics obtained when these data are included are provided as supplementary materials.

Southern Ocean	phosphate	nitrate	silicate	oxygen	TA	pH	DIC
N	20294	20294	20294	20294	11088	4094	11945
LIRv2	0.000 (\pm 0.059)	-0.03 (\pm 0.77)	-0.4 (\pm 5.1)	0.0 (\pm 6.3)	-0.3 (\pm 3.3)	-0.001 (\pm 0.011)	-
ESPER_LIR	-0.004 (\pm 0.062)	-0.07 (\pm 0.76)	0.1 (\pm 4.8)	0.0 (\pm 6.3)	0.3 (\pm 3.0)	-0.001 (\pm 0.013)	1.4 (\pm 4.7)
ESPER	-0.003 (\pm 0.054)	-0.03 (\pm 0.69)	0.0 (\pm 3.9)	0.6 (\pm 6.1)	0.7 (\pm 3.1)	-0.002 (\pm 0.010)	1.6 (\pm 4.6)
CANYON-B	-0.001 (\pm 0.055)	-0.04 (\pm 0.65)	0.1 (\pm 3.7)	†	-0.4 (\pm 3.1)	-0.002 (\pm 0.009)	-0.8 (\pm 4.3)
ESPER Mixed	-0.003 (\pm 0.057)	-0.05 (\pm 0.71)	0.1 (\pm 4.1)	0.3 (\pm 5.8)	0.5 (\pm 2.9)	-0.001 (\pm 0.011)	1.5 (\pm 4.6)
Equatorial Pacific	phosphate	nitrate	silicate	oxygen	TA	pH	DIC
N	23169	23169	23169	23169	8661	1739	8969
LIRv2	-0.003 (\pm 0.038)	0.04 (\pm 0.54)	0.1 (\pm 1.2)	0.7 (\pm 4.6)	0.8 (\pm 3.5)	-0.012 (\pm 0.016)	-
ESPER_LIR	-0.002 (\pm 0.041)	0.09 (\pm 0.56)	0.3 (\pm 1.4)	1.0 (\pm 4.7)	0.9 (\pm 3.3)	-0.007 (\pm 0.017)	-0.8 (\pm 5.1)
ESPER	-0.003 (\pm 0.033)	0.05 (\pm 0.37)	0.3 (\pm 1.3)	0.2 (\pm 3.9)	1.0 (\pm 3.4)	-0.007 (\pm 0.014)	-0.5 (\pm 5.2)
CANYON-B	-0.003 (\pm 0.033)	0.04 (\pm 0.38)	0.2 (\pm 1.2)	†	0.1 (\pm 4.4)	-0.004 (\pm 0.011)	-1.3 (\pm 5.1)
ESPER Mixed	-0.003 (\pm 0.034)	0.07 (\pm 0.43)	0.3 (\pm 1.3)	0.6 (\pm 3.9)	1.0 (\pm 3.2)	-0.007 (\pm 0.014)	-0.6 (\pm 5.0)
California Current	phosphate	nitrate	silicate	oxygen	TA	pH	DIC
N	466	466	466	466	283	191	276
LIRv2	-0.012 (\pm 0.049)	0.02 (\pm 0.79)	-0.8 (\pm 3.3)	0.4 (\pm 9.0)	2.2 (\pm 3.8)	-0.008 (\pm 0.012)	-
ESPER_LIR	-0.004 (\pm 0.046)	0.00 (\pm 0.75)	-0.2 (\pm 2.4)	0.6 (\pm 8.2)	2.3 (\pm 4.9)	-0.007 (\pm 0.015)	-0.3 (\pm 4.5)
ESPER	0.002 (\pm 0.044)	-0.02 (\pm 0.55)	0.7 (\pm 1.7)	0.5 (\pm 5.6)	3.0 (\pm 4.3)	-0.004 (\pm 0.011)	1.2 (\pm 4.6)
CANYON-B	-0.006 (\pm 0.042)	0.04 (\pm 0.58)	0.0 (\pm 1.9)	†	3.6 (\pm 5.2)	-0.002 (\pm 0.010)	1.3 (\pm 5.1)
ESPER Mixed	-0.001 (\pm 0.042)	-0.01 (\pm 0.54)	0.3 (\pm 1.7)	0.5 (\pm 5.6)	2.7 (\pm 4.1)	-0.006 (\pm 0.012)	0.5 (\pm 4.1)
Northern Atlantic	phosphate	nitrate	silicate	oxygen	TA	pH	DIC
N	10829	10829	10829	10829	6619	1123	4743
LIRv2	0.009 (\pm 0.070)	0.14 (\pm 1.16)	0.3 (\pm 2.5)	0.7 (\pm 9.8)	-0.6 (\pm 6.3)	0.003 (\pm 0.010)	-
ESPER_LIR	0.006 (\pm 0.071)	0.05 (\pm 1.23)	0.3 (\pm 1.2)	0.6 (\pm 9.2)	-0.7 (\pm 5.0)	-0.003 (\pm 0.011)	1.0 (\pm 7.7)
ESPER	0.009 (\pm 0.069)	0.12 (\pm 0.99)	0.3 (\pm 1.0)	0.1 (\pm 7.7)	-1.0 (\pm 5.4)	-0.004 (\pm 0.009)	0.9 (\pm 8.3)
CANYON-B	0.012 (\pm 0.067)	0.09 (\pm 1.02)	0.2 (\pm 1.1)	†	-0.3 (\pm 5.7)	-0.004 (\pm 0.008)	-1.0 (\pm 8.6)

<u>ESPER</u> Mixed	0.008 (\pm 0.067)	0.09 (\pm 1.05)	0.3 (\pm 1.0)	0.4 (\pm 8.2)	-0.8 (\pm 5.0)	-0.003 (\pm 0.009)	1.0 (\pm 7.7)
Sea of Japan/East Sea	phosphate	nitrate	silicate	oxygen	TA	pH	DIC
N	5995	5995	5995	5995	1450	0	1480
LIRv2	0.431 (\pm 0.459)	6.20 (\pm 6.90)	46.2 (\pm 54.6)	-19.1 (\pm 63.2)	-31.7 (\pm 209.3)	*	-
<u>ESPER</u> LIR	0.101 (\pm 0.154)	1.63 (\pm 2.11)	3.0 (\pm 7.7)	6.6 (\pm 15.5)	51.4 (\pm 63.0)	*	2.2 (\pm 17.2)
<u>ESPER</u>	0.029 (\pm 0.066)	1.16 (\pm 1.58)	3.6 (\pm 4.6)	5.4 (\pm 10.3)	48.7 (\pm 55.5)	*	16.8 (\pm 20.0)
CANYON-B	0.385 (\pm 0.409)	5.88 (\pm 6.42)	21.0 (\pm 23.6)	†	28.3 (\pm 33.8)	*	12.3 (\pm 18.4)
<u>ESPER</u> Mixed	0.065 (\pm 0.094)	1.40 (\pm 1.66)	3.3 (\pm 5.3)	6.0 (\pm 10.8)	50.0 (\pm 58.8)	*	9.5 (\pm 14.2)
Gulf of Mexico	phosphate	nitrate	silicate	oxygen	TA	pH	DIC
N	1067	1067	1067	1067	943	0	909
LIRv2	-0.004 (\pm 0.123)	0.27 (\pm 1.71)	0.5 (\pm 3.8)	8.6 (\pm 16.1)	-0.9 (\pm 11.4)	*	-
<u>ESPER</u> LIR	-0.009 (\pm 0.110)	0.30 (\pm 1.58)	-0.3 (\pm 2.1)	6.6 (\pm 16.6)	-16.3 (\pm 44.5)	*	-8.7 (\pm 26.1)
<u>ESPER</u>	0.002 (\pm 0.108)	0.35 (\pm 1.39)	1.0 (\pm 3.4)	7.3 (\pm 16.5)	-27.5 (\pm 47.4)	*	-19.6 (\pm 41.6)
CANYON-B	0.056 (\pm 0.125)	0.68 (\pm 1.40)	2.5 (\pm 5.2)	†	4.5 (\pm 13.0)	*	-5.1 (\pm 16.8)
<u>ESPER</u> Mixed	-0.003 (\pm 0.099)	0.32 (\pm 1.38)	0.4 (\pm 2.4)	7.0 (\pm 15.8)	-21.9 (\pm 45.1)	*	-14.2 (\pm 33.4)
Mediterranean	phosphate	nitrate	silicate	oxygen	TA	pH	DIC
N	11394	11394	11394	11394	5164	0	2604
LIRv2	0.081 (\pm 0.254)	1.90 (\pm 4.85)	0.5 (\pm 7.3)	-10.4 (\pm 50.0)	-37.9 (\pm 71.2)	*	-
<u>ESPER</u> LIR	0.003 (\pm 0.585)	2.44 (\pm 7.72)	-4.0 (\pm 37.5)	-25.1 (\pm 92.5)	-43.9 (\pm 72.1)	*	-105.9 (\pm 169.9)
<u>ESPER</u>	0.095 (\pm 0.199)	-2.40 (\pm 6.21)	-28.6 (\pm 40.1)	1.8 (\pm 15.3)	-30.0 (\pm 43.9)	*	-40.7 (\pm 48.9)
CANYON-B	*	*	*	†	*	*	-3.0 (\pm 26.2)
<u>ESPER</u> Mixed	0.049 (\pm 0.325)	0.02 (\pm 4.82)	-16.3 (\pm 30.2)	-11.6 (\pm 45.7)	-37.0 (\pm 54.3)	*	-73.3 (\pm 101.6)
Arctic	phosphate	nitrate	silicate	oxygen	TA	pH	DIC
N	6117	6117	6117	6117	3189	1634	2947
LIRv2	0.036 (\pm 0.122)	0.28 (\pm 1.20)	0.5 (\pm 3.4)	2.7 (\pm 11.8)	1.5 (\pm 19.4)	*	-
<u>ESPER</u> LIR	0.043 (\pm 0.121)	0.25 (\pm 1.22)	0.4 (\pm 2.9)	3.3 (\pm 11.4)	0.0 (\pm 12.7)	0.003 (\pm 0.032)	-1.0 (\pm 18.7)
<u>ESPER</u>	0.022 (\pm 0.104)	0.19 (\pm 0.95)	0.0 (\pm 2.3)	1.9 (\pm 11.1)	-2.9 (\pm 13.3)	0.021 (\pm 0.054)	-2.6 (\pm 16.0)
CANYON-B	*	*	*	*	*	*	*
<u>ESPER</u> Mixed	0.033 (\pm 0.099)	0.22 (\pm 1.00)	0.2 (\pm 2.3)	2.6 (\pm 10.8)	-1.5 (\pm 11.5)	0.012 (\pm 0.037)	-1.8 (\pm 16.4)

*No viable comparison in this effort due to partial or complete overlap between training and validation data subsets or insufficient viable measurements

†This routine does not estimate this quantity.

